AIP Physics of Fluids

Reynolds number influence on statistical behaviors of turbulence in a circular free jet

J. Mi, M. Xu, and T. Zhou

Citation: Physics of Fluids (1994-present) **25**, 075101 (2013); doi: 10.1063/1.4811403
View online: http://dx.doi.org/10.1063/1.4811403
View Table of Contents: http://scitation.aip.org/content/aip/journal/pof2/25/7?ver=pdfcov
Published by the AIP Publishing

PHYSICS OF FLUIDS **25**, 075101 (2013)

Reynolds number influence on statistical behaviors of turbulence in a circular free jet

J. Mi,[1,2,a)] M. Xu,[1,3] and T. Zhou[4]
[1]*State Key Laboratory of Turbulence and Complex Systems and Department of Energy and Resources Engineering, College of Engineering, Peking University, Beijing 100871, China*
[2]*College of Energy and Power Engineering, Changsha University of Science and Technology, Changsha 410004, China*
[3]*Marine Engineering College, Dalian Maritime University, Dalian 116026, China*
[4]*School of Civil and Resource Engineering, University of Western Australia, WA 6009, Australia*

(Received 28 January 2013; accepted 17 May 2013; published online 8 July 2013)

The present paper examines the effect of Reynolds number on turbulence properties in the transition region of a circular jet issuing from a smoothly contracting nozzle. Hot-wire measurements were performed for this investigation through varying the jet-exit Reynolds number Re_d ($\equiv U_j d/\nu$, where U_j, d, and ν are the jet-exit mean velocity, nozzle diameter, and kinematic viscosity) approximately from $\mathrm{Re}_d \approx 4 \times 10^3$ to $\mathrm{Re}_d \approx 2 \times 10^4$. Results reveal that the rates of the mean flow decay and spread vary with Reynolds number for $\mathrm{Re}_d < 10^4$ and tend to become Reynolds-number independent at $\mathrm{Re}_d \geq 10^4$. Even more importantly, the small-scale turbulence properties, e.g., the mean rate of dissipation of kinetic energy (ε), the Kolmogorov and Taylor microscales, are found to vary in different forms over the Re_d ranges of $\mathrm{Re}_d > 10^4$ and $\mathrm{Re}_d < 10^4$. Namely, the critical Reynolds number appears to occur at $\mathrm{Re}_{d,cr} \approx 10^4$ across which the jet turbulence behaves distinctly. Two turbulence regimes are therefore identified: (i) developing or partially developed turbulence at $\mathrm{Re}_d < \mathrm{Re}_{d,cr}$ and (ii) fully developed turbulence at $\mathrm{Re}_d \geq \mathrm{Re}_{d,cr}$. It is suggested that the energy dissipation rate (DR) can be expressed as $\varepsilon \sim \nu U_c^2/R^2$ in regime (i) and $\varepsilon \sim U_c^3/R$ in regime (ii), where U_c and R are the centerline (or maximum) mean velocity and half-radius at which the mean velocity is $0.5U_c$. In addition, the critical Reynolds number appears to vary from flow to flow. © *2013 AIP Publishing LLC*. [http://dx.doi.org/10.1063/1.4811403]

I. INTRODUCTION

Turbulent jets are widely used in various mixing processes of industry such as combustion and pollution dispersal. In these flows, large-scale motions contain most of the energy and play a dominant role in transfers of momentum, heat, and mass, while the small-scale turbulence brings different species together at the molecular level, see, e.g., Refs. 1–3. Note that the small-scale turbulence spans the dissipative and inertial ranges, which refers to the case for fully turbulent flows corresponding to sufficiently high Reynolds numbers; inertial-range scales are large compared to dissipative scales but small compared to the global flow scales. There is no difficulty in defining these scale-ranges formally at high Reynolds numbers (e.g., Refs. 4 and 5), but their precise definitions are always difficult at small to moderate Reynolds numbers.[1]

It has become well known that statistical behaviors of both large-scale and small-scale turbulent motions in jets depend upon the initial inflow conditions (e.g., Refs. 6–23). Among them, the

[a)]Author to whom correspondence should be addressed. Electronic mail: jcmi@coe.pku.edu.cn. Telephone: +86 10 6276 7074.

Reynolds number defined by $\mathrm{Re}_d \equiv U_j d/\nu$ (where U_j, d, and ν are the jet-exit mean velocity, circular nozzle diameter or non-circular nozzle equivalent diameter, and kinematic viscosity) is perhaps the most important quantified condition. Although the influence of Re_d on the downstream development of a turbulent jet has been investigated extensively, in terms of large-scale global properties (e.g., Refs. 10–23), this topic remains as an interesting challenge, particularly, with respect to those issues related to the small-scale turbulence.

There have been quite a number of previous studies investigating the Re_d effect on a circular turbulent jet issuing from a smooth contraction (SC) nozzle with a top-hat or nearly uniform mean velocity at exit. Ricou and Spalding[10] investigated the Re_d effect on the entrainment ratio ($\equiv$ entrained mass flow rate/jet exit mass flow rate) over the Reynolds number range $500 \le \mathrm{Re}_d \le 8 \times 10^4$ in their preliminary experiments. These authors found that the ratio was approximately constant for $\mathrm{Re}_d > 2 \times 10^4$–$2.5 \times 10^4$. They then chose to carry out the remainder of their experiments for $\mathrm{Re}_d \ge 2.5 \times 10^4$. Dimotakis *et al.*[11] assessed the scalar-mixing fields of the circular SC jets at $\mathrm{Re}_d = 2.5 \times 10^3$–$10^4$ and found a particular transition in turbulent mixing behavior for Re_d on the order of 10^4. Miller and Dimotakis[12] confirmed that the root-mean-squared (RMS) scalar fluctuations in a water-to-water SC jet decrease with increasing Re_d and converge to an asymptotic state at $\mathrm{Re}_d \approx 2.0 \times 10^4$, which is a homogeneous, chaotic, and well-mixed state. Likewise, Gilbrech[13] found that the asymptotic state of the mixing field occurs at $\mathrm{Re}_d \approx 2.0 \times 10^4$. Koochesfahani and Dimotakis[14] used scalar images of laser-induced fluorescence (LIF) at $\mathrm{Re}_d = 1.75 \times 10^3$ and 2.30×10^4 and showed qualitatively a better-mixed state at the larger Re_d. Similarly, Michalke[15] found that the growth of instability waves in jet shear layers can be reduced dramatically when Reynolds number is increased. Oosthuizen[16] measured a circular SC jet at low Reynolds numbers and found that both the mean and fluctuating fields depend strongly on Re_d for $\mathrm{Re}_d < 10^4$. Using large eddy simulation (LES), Bogey and Bailly[17] modeled a circular jet at $\mathrm{Re}_d = 1.70 \times 10^3$–$4.0 \times 10^5$ and showed that, as Re_d is decreased, the jet develops more slowly within the potential core, but more rapidly farther downstream. Their circular jets achieve self-preservation at a location closer to the exit plane at low values of Re_d, a finding which agrees well with that of Pitts[18] for turbulent circular SC jets measured for $\mathrm{Re}_d = 3950$–$11\,880$. Moreover, Panchapakesan and Lumley[19] and Hussein *et al.*[20] indicated that at sufficiently high Reynolds numbers, the decay and spread rates of the SC jet should be approximately independent of Re_d, but they did not measure the flow at different values of Re_d and so did not indicate a critical Reynolds number, Re_{cr}, above which this independence occurs. Pope[21] has nevertheless made it clear in his text that the mean velocity profile and the spreading rate are independent of Re_d in the self-similar region ($x/d > 30$, where x is the downstream distance from the nozzle exit) of a high-Reynolds number turbulent jet ($\mathrm{Re}_d > 10^4$). This value of Re_d ($=10^4$) is more or less identical to that suggested by Dimotakis[4,24] for the critical Reynolds number at which turbulent "mixing transition" starts. He claimed that the fully developed turbulent flow requires an outer-scale Reynolds number of 1.0×10^4–2.0×10^4 or a Taylor Reynolds number of 100–140 to be sustained and thus suggested that "turbulent flow below this Reynolds number cannot be regarded as fully developed and can be expected to be qualitatively different." Dimotakis[24] also explained the turbulent mixing transition based on the relative magnitudes of dimensional spatial scales of flow.

However, to our best knowledge, apart from some experimental investigations of Antonia *et al.*[25,26] and Fellouah and Pollard,[27] there have been no other studies, especially systematic detailed ones, available on the Re_d dependences of the small-scale turbulence properties of a circular jet and other shear flows. Despite this, some experimental studies into grid turbulences, e.g., Batchelor[4] and Sreenivasan,[28] were carried out to test the long-held belief that the time scale of the dissipation rate in fully turbulent flows is of the same order of magnitude as the characteristic time scale of the energy containing eddies. Also, the Reynolds-number effect was extensively investigated on the skewness and flatness factors of the velocity streamwise derivatives transformed from the temporal derivatives in 1960-1980s, as detailed in Sreenivasan and Antonia[1] and Van Atta and Antonia.[29] Antonia *et al.*[25] reported the centerline variations of several characteristic quantities of small-scale turbulence, i.e., the mean dissipation rate ε, the Kolmogorov length scale $\eta \equiv (\nu^3/\varepsilon)^{1/4}$, the Taylor micro-scale $\lambda \equiv \langle u^2\rangle^{1/2}\langle(\partial u/\partial x)^2\rangle^{-1/2}$, and the turbulence Reynolds number $\mathrm{Re}_\lambda = \langle u^2\rangle^{1/2}\lambda/\nu$; here u represents the longitudinal component of the fluctuating velocity. Their measurements were made in both circular and plane jets. These authors also obtained the relationship between Re_λ and Re_d, which is $\mathrm{Re}_\lambda \approx 1.74\mathrm{Re}_d^{1/2}$. However, they used only three relatively high values of Re_d ($=5.56 \times 10^4$, 1.09×10^5, and 4.71×10^5) for the circular jet and two (2.04×10^4, 4.28×10^4) for the plane jet and did not consider low Reynolds number effect. Very recently, Fellouah and Pollard[27] measured η, λ, and also the outer laminar thickness and inner viscous scale[24] at different positions in near to intermediate regions of a circular free jet for the purpose to investigate the concept of a mixing transition proposed by Dimotakis.[24] They found that all these scales decrease in magnitude with the local Reynolds number based on the local centerline mean velocity and the local time-averaged diameter of the jet but appear to be nearly constant across the jet, which is unexpected. Note that five different values of their Reynolds number Re_d were taken between 6×10^3 and 1.0×10^5; unfortunately, however, only one value of Re_d was below 10^4. In this context, there have been insufficient data for low Reynolds numbers available to determine reliably either the scale factors of ε, η, λ, and Re_λ or the critical value of Re_d which draws up a distinct boundary between low and high Reynolds number regimes or around which a turbulent mixing transition just occurs.

To address the above lack, the present study is aimed at investigating the Re_d dependences of both the global properties (e.g., the mean velocity decay and spread rates: K_U and K_R) and small-scale turbulence properties (e.g., ε, η, λ, and Re_λ) in the transition and early far-field regions of a circular jet at eight different Reynolds numbers between $\mathrm{Re}_d \approx 0.4 \times 10^4$ and $\mathrm{Re}_d \approx 2.0 \times 10^4$. More specifically, the investigation is aimed at

(1) quantifying the Re_d dependences of the global properties K_U, K_R, and the small-scale properties ε, η, λ, and Re_λ;
(2) identifying the critical Reynolds number based on both large and small-scale flow properties; and
(3) clarifying the way in which ε scales, particularly for low Re_d, with relatively easily measureable characteristic velocity and length scales.

To the above end, detailed measurements of the fluctuating velocity over a downstream distance of about 30 nozzle exit diameters, crossing the near-field, transition, and far-field regions, were performed by varying Re_d systematically between 4×10^3 and 2×10^4, a range of Re_d which is believed to span the mixing transition across the critical Reynolds number.[2,24] The digital filter scheme proposed by Mi *et al.*[30] and recently validated further by Mi *et al.*[31] was employed to obtain likely good-quality data of small-scale turbulence.

The rest of the paper is arranged as below. In Sec. II, the self-preserving relations are analytically derived for ε, η, λ, and Re_λ which are dependent on Re_d. Details of experiments and data processing are then provided in Sec. III that includes the measurement procedure, hotwire resolution and correction, post-filtering scheme, and initial mean and RMS velocity profiles. Basic large-scale properties (e.g., mean and RMS velocities) are presented in Sec. IV whereas small-scale properties of turbulence for the circular jet are analyzed in Sec. V. In Sec. VI, further discussion about turbulence mixing transition is given. Concluding remarks are finally provided in Sec. VII.

II. SELF-PRESERVING RELATIONS OF THE Re_d-DEPENDENT ε, η, λ, AND Re_λ

In the far field of a circular jet, the mean velocity field is expected to approach self-preservation which requires the centerline mean velocity U_c as the characteristic velocity scale and the half-radius R as the characteristic length scale to obey the following equations (e.g., Ref. 21):

$$U_c/U_j = K_U[(x - x_U)/d]^{-1}, \tag{1}$$

$$R/d = K_R[(x - x_R)/d]. \tag{2}$$

Here, K_U and K_R are the jet velocity decay constant and spread rate, respectively, while x is the streamwise coordinate or downstream distance measured from the nozzle exit; x_U and x_R are the x-locations of the virtual origin of (1) and (2). Further, if the fluctuating velocity field also asymptotes to self-preservation, each component of the centerline RMS velocity divided by U_c, i.e., the turbulence intensity, should be constant in the far field; e.g., the streamwise component

$$\langle u^2\rangle^{1/2} U_c = K_I \tag{3}$$

should not vary with x.

For turbulent jets of low Reynolds numbers, both the mean and fluctuating fields are expected to depend strongly on Re_d, and the energy-containing range and that of the dissipation overlap (e.g., Tennekes and Lumley[32]). So there must be viscous effects in the process of energy transferring from large eddies to small eddies and thus dimensional analysis leads to the energy dissipation rate being expressed by the characteristic scales (U_c, R) as

$$\varepsilon = K_{\varepsilon l} \nu U_c^2/R^2, \tag{4}$$

where $K_{\varepsilon l}$ is an experimental constant, independent of Reynolds number. On the other hand, when Re_d is sufficiently high, K_U, K_R, and K_I are nearly independent of Re_d (e.g., Ref. 21). It is considered that ε should be equal to the supply rate of the turbulence kinetic energy from the large-scale structures (e.g., Ref. 32), which is of order U_c^3/R, i.e.,

$$\varepsilon = K_{\varepsilon h} U_c^3/R \tag{5}$$

and $K_{\varepsilon h}$ is a Re_d-independent constant. It is worth noting that Eq. (5) actually can be derived from three apparently independent arguments generally for any turbulent flows, where U_c and R are treated as characteristic scales in general. These arguments follow. In Kolmogorov's equilibrium hypothesis,[33] it is assumed that the turbulence dynamics in the non-dissipative scales depend only upon the energy flux and the length scale. Following this, Laudau and Lifshitz[34] demonstrated that Eq. (5) is a simple consequence of dimensional analysis. According to Townsend,[35] Eq. (5) is obtained because it is a necessary condition for free turbulent flows to achieve the self-preserving state. Moreover, assuming the rate of energy supply by large eddies to small eddies to be inversely proportional to the time scale of the large eddies, i.e., $\langle u^2\rangle^{-1} d\langle u^2\rangle/dt \sim U_c/R$, we can easily obtain that $\varepsilon \sim d\langle u^2\rangle/dt \sim U_c^3/R$, which is Eq. (5). Note that Eq. (5) has been well validated by a number of previous investigations in several turbulent flows, e.g., Refs. 25 and 26; however, to our best knowledge, perhaps Eq. (4) has yet to be checked in detail in any turbulent flows.

Substituting (1) and (2) either into (4) or (5) can enable the normalized dissipation rate, assuming that $x_U = x_R$, to be expressed as

$$\varepsilon^* = \varepsilon(d/U_j^3) = C_\varepsilon[(x - x_\varepsilon)/d]^{-4} \tag{6}$$

in the self-preserving circular jet. That is, Eq. (6) works for a round turbulent jet at any relevant Re_d. The first derivation of Eq. (6) was perhaps made by Friehe *et al.*[36] for high Reynolds numbers. In (6), C_ε and x_ε denote the prefactor and the virtual origin location, respectively, perhaps both depending on Re_d. The value of C_ε can be determined by substituting measured data into (6) or by the following equations over two regimes of turbulence, i.e.,

$$\text{Regime (i)}: \quad C_{\varepsilon l} = K_{\varepsilon l} K_U^2 K_R^{-2} \mathrm{Re}_d^{-1} \quad \text{at } \mathrm{Re}_d < \mathrm{Re}_{cr}, \tag{7a}$$

$$\text{Regime (ii)}: \quad C_{\varepsilon h} = K_{\varepsilon h} K_U^3 K_R^{-1} \quad \text{at } \mathrm{Re}_d \geq \mathrm{Re}_{cr}. \tag{7b}$$

Both $K_{\varepsilon l}$ and $K_{\varepsilon h}$ are independent of Re_d. Similarly, several characteristic turbulence scales, such as the Kolmogorov length scale $\eta \equiv (\nu^3/\varepsilon)^{1/4}$, the Taylor micro-scale $\lambda \equiv \langle u^2\rangle^{1/2}\langle(\partial u/\partial x)^2\rangle^{-1/2}$ and the turbulence Reynolds number $\mathrm{Re}_\lambda = \langle u^2\rangle^{1/2}\lambda/\nu$ can be analytically expressed as (assuming the isotropic turbulence, i.e., $\varepsilon = 15\nu\langle(\partial u/\partial x)^2\rangle$)

$$\eta/d = C_\eta[(x - x_\eta)/d] \quad \text{with} \quad C_\eta = C_\varepsilon^{-1/4}\,\mathrm{Re}_d^{-3/4}, \tag{8}$$

$$\lambda/d = C_\lambda[(x - x_\lambda)/d] \quad \text{with} \quad C_\lambda = \sqrt{15} K_I K_U C_\varepsilon^{-1/2}\,\mathrm{Re}_d^{-1/2}, \tag{9}$$

$$\mathrm{Re}_\lambda = C_{\mathrm{Re}} \mathrm{Re}_d^{1/2} \quad \text{with} \quad C_{\mathrm{Re}} = \sqrt{15} K_I^2 K_U^2 C_\varepsilon^{-1/2}. \tag{10}$$

In Eqs. (8)–(10), C_ε represents both $C_{\varepsilon l}$ and $C_{\varepsilon h}$ for convenience; this implies that the Re_d dependences of C_η and C_λ occur over both regimes whereas that of C_{Re} takes place only in regime (i) at $\mathrm{Re}_d < \mathrm{Re}_{cr}$. They may be determined by the measured data of η and λ through Eqs. (8)–(10) or by constants K_U, K_R, K_I, $K_{\varepsilon h}$, and $K_{\varepsilon l}$ obtained from measurements of the mean velocity and the centerline fluctuating velocity. In addition, the virtual origin locations x_η and x_λ are expected to be different from their counterparts for Eqs. (1), (2), and (6) as will be indicated late in Sec. V D.

III. EXPERIMENTAL DETAILS AND DATA PROCESSING METHODS

A. Experimental setup and procedure

The present circular jets were generated from a nozzle system whose schematic diagram is shown in Fig. 1. The facility consists of a cylindrical plenum chamber with an internal diameter of 95 mm and a length of 600 mm. Filtered and compressed air is supplied through the plenum to a smooth contraction nozzle. The nozzle outlet profile is third-order polynomial, contracting from a diameter of 95 mm to the exit diameter of $d = 20$ mm, flush with a flat surface of 200 mm in diameter. This enables the exit profile of the mean velocity to be "top-hat"-shaped, i.e., uniform except for the shear layer region near the edge of the nozzle. The exit velocity U_j was varied over the range $3 \le U_j \le 15$ m/s, corresponding to the Reynolds number $\mathrm{Re}_d \approx 4050$–20 100. In addition, the jet facility was horizontally placed in a room of dimensions 9600 mm × 6000 mm × 3500 mm, with the nozzle locating at a height of 1500 mm (75d) above the floor and the nozzle exit being more than 300d away from the wall. It is thus assumed that, according to Hussein *et al.*,[20] the present measurements conducted in such a confined laboratory would suffer from negligible loss of momentum with increasing downstream distance.

Present velocity measurements were performed using hot-wire anemometer mainly along the centerline at $x/d \le 30$, where x is the downstream distance measured from the nozzle exit. Only the streamwise component of the instantaneous velocity was taken by a single hot-wire (tungsten) probe, operated by an in-house constant temperature circuit with overheat ratio of 1.5. The hot-wire sensor, aligned perpendicular to the x-axis, is 5 μm in diameter (d_w) and approximately 1.0 mm in length (l_w) so that $l_w/d_w \approx 200$. It was normally suggested that $l_w/d_w \ge 200$ so as to enable the central portion of the wire to have a uniform temperature distribution (e.g., Hinze[37]). For the present experimental conditions, the frequency response of the hot wire and anemometer, determined by the square-wave technique, was about 100 kHz, so that the temporal response of the wire was approximately 10^{-5} s. To avoid the aerodynamic interference of prongs on the hot-wire sensor, the present probe was carefully mounted, with prongs parallel to the circular jet exit.

It is worth noting that Mi and Antonia[38] performed measurements of the mean and RMS velocities, as well as those of their lateral gradients, using single-wire and one or four X-wire

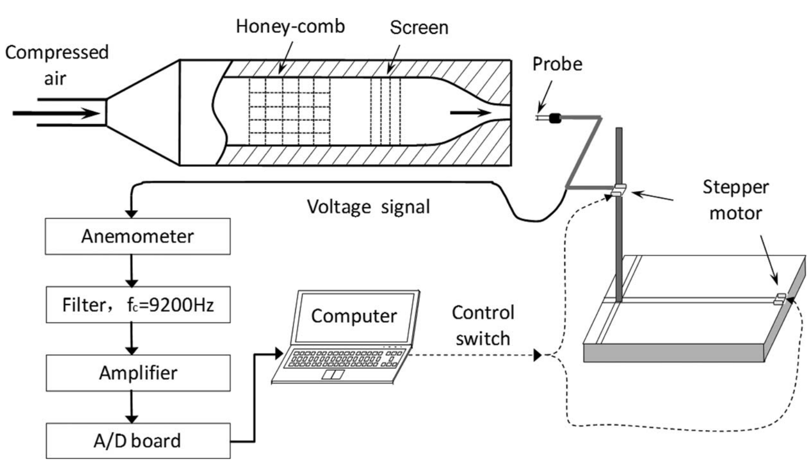

FIG. 1. A schematic diagram of the experimental arrangement.

probes, in the turbulent wake of a circular cylinder. These authors demonstrated that the single-wire probe measured the streamwise velocity appropriately in the wake flow at $x/d = 20$ (here d is the cylinder diameter), obtaining nearly the same results as from X-wire probes (see their Figs. 2 and 5). The flow under the present consideration was not more highly three-dimensional than the wake flow of Mi and Antonia.[38] Accordingly, we are confident that the experimental data from the present single-wire measurements should not lead to generally wrong conclusions.

Calibrations of the hot-wire were conducted, prior to and after each set of measurements, using a standard static Pitot tube located side by side with the probe in the potential core of the jet, where the velocity field is nearly uniform over the space occupied by the sensor and prongs. For each U_j or Re_d, different ranges of velocity were used in calibration from 0.5–3 m/s to 0.5–15 m/s. The calibration data were well fit using either the 3rd polynomial (preferred) or King's law, which virtually resulted in nearly identical velocity results. Instantaneous velocity signals obtained were low-pass filtered with an identical cutoff frequency of $f_c = 9.2$ kHz, the maximum value set by the anemometer, for all measurements to eliminate excessively high-frequency noise (see Sec. III B for a detailed filtering process) and also to avoid any aliasing. To obtain the maximum possible signal-to-noise ratio, the mean voltages were sampled and removed from the signals by means of the offset and the remaining fluctuations were amplified by a factor of 3–6 before they were sampled. Then the voltage signals set within (0–3) voltages were amplified appropriately through circuits. They were digitized on a personal computer at $f_s = 18.4$ kHz (versus the hot-wire response frequency ≈ 100 kHz) via a 12 bit A/D converter and each record had duration of about 30 s. In addition, the control of hot-wire position and data acquisition was accomplished using the National Instruments software LabVIEW, as indicated in Fig. 1.

B. Limited hotwire spatial and temporal resolutions and their corrections

The present hotwire probe has a limited overall resolution due to its finite spatial dimensions and temporal response. Specifically, the spatial resolution was determined by the wire diameter $d_w = 5\ \mu$m and effective length $\ell_w \approx 1$ mm, while the temporal resolution depended upon the sampling rate $f_s = 18.4$ kHz. Note that the ratio $\ell_w/d_w \approx 200$ is required so that both a nearly uniform temperature distribution in the central portion of the wire and a high sensitivity to flow velocity fluctuations can be achieved.[37,38] The present study corrected the spatial attenuation of the single wire due to $\ell_w \approx 1$ mm using the procedure of Wyngaard,[39] which was developed in spectral space to account for the ℓ_w integration effect on Fourier components of the velocity. A very brief description is given below.

The one-dimensional energy spectra, $\Phi^w(k_1)$ and $\Phi^{nw}(k_1)$, of the measured fluctuating velocity subject to the wire-length effect or not can be expressed, respectively, as

$$\Phi^{nw}(k_1) = \int_{-\infty}^{\infty}\int_{-\infty}^{\infty} E(\mathbf{k})dk_2dk_3 \tag{11}$$

and

$$\Phi^{w}(k_1) = \int_{-\infty}^{\infty}\int_{-\infty}^{\infty} [\sin^2(\tfrac{1}{2}k_2\ell_{\mathrm{w}})/(\tfrac{1}{2}k_2\ell_{\mathrm{w}})^2]E(\mathbf{k})dk_2dk_3, \tag{12}$$

where $\mathbf{k}$ is the wavenumber vector with streamwise, lateral, and spanwise components k_1, k_2, and k_3; $|\mathbf{k}| = k = \sqrt{k_1^2 + k_2^2 + k_3^2}$. For isotropic turbulence, Φ is related to $E(k)$ by the relation

$$\Phi\,(k) = \Phi\,(k) = E\,(k)\left(k_2^2 + k_3^2\right)/(4\pi k^2),$$

see Ref. 37. Following Antonia and Mi,[40] we use a relatively simple and convenient approach to derive $E(k)$ from $\Phi^w(k_1)$ via the well-known isotropic relation

$$E(k) = k^2\left(\frac{\partial^2\Phi^w}{\partial k_1^2}\right)_{k_1=k} - k\left(\frac{\partial\Phi^w}{\partial k_1}\right)_{k_1=k}. \tag{13}$$

The resulting distribution of $E(k)$ can then be utilized as input for Eqs. (11) and (12). This procedure takes into account the effect of the wire length through the ratio $\Phi^w(k_1)/\Phi^{nw}(k_1)$ which is applied to the spectral content of the velocity and, consequently, the energy dissipation rate estimated by the local isotropic form $\varepsilon = 15\nu\langle(\partial u/\partial x)^2\rangle$. In general, the correction for the u-RMS, $\langle u^2\rangle^{1/2}$, due to spatial attenuation of $\ell_w \approx 1$ mm is within 1.3% of all the original data and that of ε is from 12% to 1.6% for $\mathrm{Re}_d = 4050$ and from 48% to 9% for $\mathrm{Re}_d = 20\,100$ over the range of $x/d = 19$–33.

Next, we consider the correction of the measured $\varepsilon = 15\nu\langle(\partial u/\partial x)^2\rangle$, where $\partial u/\partial x \approx -U^{-1}\partial u/\partial t \approx -U^{-1}[u(t+\Delta t) - u(t)]/\Delta t = [u(t + f_s^{-1}) - u(t)] f_s$ based on the Taylor's hypothesis. This correction is for the temporal resolution of $\Delta t = f_s{}^{-1}$ due to the limited sampling rate of $f_s = 18.4$ kHz. Antonia and Mi[40] found that the assumption of local isotropy and an assumed form for $E(k)$, seen in Eq. (13), are not necessary for correcting the measured $\langle(\partial u/\partial x)^2\rangle_m$. Accordingly, the corrected streamwise derivative for the present case may be expressed as[40,41]

$$\left\langle(\partial u/\partial x)^2\right\rangle_{corr} = \int_0^\infty \frac{(k_1\Delta x/2)^2}{\sin^2(k_1\Delta x/2)}\Phi^m_{\partial u/\partial x}(k_1)dk_1 = \int_0^\infty \frac{(k_1\Delta x/2)^2}{U^2\sin^2(k_1\Delta x/2)}\Phi^m_{\partial u/\partial t}(k_1)dk_1,$$

where $\Delta x = U\Delta t = U f_s^{-1}$ and $k_1 = 2\pi f U^{-1}$. Note that $\Phi^m_{\partial u/\partial t}(f)$ is directly measurable. We made the above corrections for $\mathrm{Re}_d \geq 10\,750$. At $\mathrm{Re}_d = 20\,100$, for instance, the streamwise distance Δx varies from 0.27 mm at $x/d = 19$ to 0.17 mm at $x/d = 33$. By comparison, the corresponding value of the Kolmogorov scale was estimated to be $\eta \approx 0.09$ mm at $x/d = 19$ to $\eta \approx 0.15$ mm at $x/d = 33$, from the corrected dissipation rates.

C. Post-filtering scheme

The present properties of small-scale turbulence were obtained using the digital scheme of filtering high-frequency noise used by Mi *et al.*[30,31] This iterative scheme obtains "true" values of η and f_K by filtering the measured velocity signal u_m, where the subscript m means "measured," based on Eqs. (11)–(13) below. Suppose that the measured dissipation rate ε_m can be expressed as

$$\varepsilon_m = \varepsilon[\text{true dissipation}] + \varepsilon_n[\text{noise contribution}] = \gamma\varepsilon \tag{14}$$

and $\gamma = (1 + \varepsilon_n/\varepsilon) > 1$. Substituting Eq. (14) into the definition of Kolmogorov scale, i.e., $\eta \equiv (\nu^3/\varepsilon)^{1/4}$, leads to

$$\eta_m = [\nu^3/(\gamma\varepsilon)]^{1/4} = \gamma^{-1/4}\eta. \tag{15}$$

It is then obtained from the Kolmogorov frequency, i.e., $f_K \equiv U/(2\pi\eta)$, where U is the streamwise mean velocity, that

$$f_{Km} = \gamma^{1/4} f_K. \tag{16}$$

The scheme iteratively uses Eqs. (14)–(16) to reduce the noise-contribution in u_m thus ε_m by filtering u_m at a new value of f_{Km}. The principle is based on the fact that the noise imposes a significantly greater influence on ε_m than on both η_m and f_{Km}. For instance, when $\varepsilon_m = 5\varepsilon$, the resulting values of η_m and f_{Km} are $\eta_m = 0.67\eta$ and $f_{Km} = 1.5 f_K$.

A great difficulty occurs in directly measuring the dissipation ε (and therefore η). The direct measurement of ε requires measurements of all 12 gradient correlations in ε (see, e.g., Refs. 21 and 37). This cannot be realized by experimental techniques available either now or in the foreseeable future. Accurate measurement of any component of ε requires a multi-sensor probe with exceptionally high spatial and temporal resolution to resolve the finest-scale or most-rapid fluctuations of velocity. In this context, the present study had to estimate ε from hot-wire measurements of $u(t)$, where $u(t)$ was substituted for $u_1(t)$ using the isotropic relation $\varepsilon = 15\nu\langle(\partial u/\partial x)^2\rangle$ together with Taylor's hypothesis $\langle(\partial u/\partial x)^2\rangle = U^{-2}\langle(\partial u/\partial t)^2\rangle$.

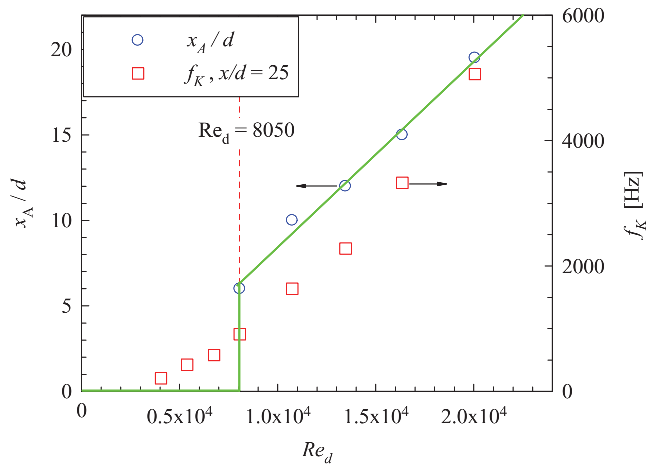

FIG. 2. Dependence on Re_d of the Kolmogorov frequency f_K for $x/d = 25$ and that of the location x_A at which $f_K = 9.2$ kHz.

In general, η decreases with increasing Re_d and increases with x, and also r, in jet flows. Correspondingly, f_K increases with Re_d and decreases with x. When Re_d is sufficiently high, there must be a particular location of $x = x_A$ at which $f_K = f_c$ (9.2 kHz). It follows that $f_K > f_c$ for $x < x_A$ where the u signals were already over-filtered at $f_c = 9.2$ kHz (no post-filtering needed) and also that $f_K < f_c$ at $x > x_A$ where u should be post-filtered necessarily at the cut-off frequency of f_K. On the other hand, for sufficiently small Re_d, f_K turns out to be smaller than f_c all along the jet centerline so that $x_A = 0$ and the post-filtering has to be taken everywhere. Indeed, as shown in Fig. 2, in the present jet, the zero value of x_A occurs at $\mathrm{Re}_d \leq 8050$ (indicated) while x_A increases with Re_d for $\mathrm{Re}_d \geq 8050$ (illustrated by a green line). Hence, the present small-scale turbulence properties shown in Sec. IV are those for $x > x_A$. In addition, Fig. 2 also shows the effect of Re_d on f_K at $x/d = 25$. Evidently, as Re_d is increased, the frequency f_K (and thus f_c) increases rapidly. Note that the subscript "m" will be removed below for simplicity.

D. Data processing method and assessment

1. Use of Taylor's hypothesis

To estimate the small-scale properties with the velocity derivatives or energy dissipation invoking the isotropic form $\varepsilon = 15\nu\langle(\partial u/\partial x)^2\rangle$, the present study had to convert time series into space series using Taylor's hypothesis, viz.,

$$\left\langle(\partial/\partial x)^2\right\rangle = U^{-2}\left\langle(\partial/\partial t)^2\right\rangle, \tag{17}$$

where U is the local mean velocity. Based on the work of Mi and Antonia,[42] the resulting data, measured along the jet centerline, were not corrected for the effect of turbulence intensity, although the relative turbulence intensity $\langle u^2\rangle/U$ is greater than 20% at $x/d > 10$ in the jet (e.g., Ref. 20). Note that in the flow of high turbulent intensity, e.g., the present flow, such a hypothesis is expected to lead to significant errors since in this situation the concept of uniform translation is not applicable. Acknowledging this, using a variety of approaches and assumptions, previous studies (e.g., Refs. 42–44) have proposed several corrections to the hypothesis, such as

$$\left\langle(\partial\theta/\partial x)^2\right\rangle = \left\langle(\partial\theta/\partial t)^2\right\rangle\left[U^2 + \left\langle u^2\right\rangle + \left\langle v^2\right\rangle + \left\langle w^2\right\rangle\right]^{-1}, \tag{18}$$

where θ denotes the fluctuating scalar; u, v, and w are the fluctuating velocity components in the streamwise, radial, and azimuthal directions, respectively. Equation (18) is strictly valid for locally isotropic turbulence. Mi and Antonia[42] checked the hypothesis (17) and several of its corrections including Eq. (18) using a passive scalar (temperature) in a circular jet ($x/d = 30$) with $\mathrm{Re}_d = 1.9 \times 10^4$. These authors found that Eq. (18) is quite closely satisfied in the fully turbulent region of the jet. They argued that the assumptions underpinning Eq. (18), i.e., homogeneity and independence between small scales and large scales, are approximately satisfied in the flow region of the investigation. Important to the present study, they also revealed that the departure from local isotropy at the level of the mean square scalar derivatives is very small along the centerline and thus that the usual form of Taylor's hypothesis, Eq. (17), is approximately valid on the jet axis, where the difference between $\langle(\partial\theta/\partial x)^2\rangle$ and $\langle(\partial\theta/\partial t)^2\rangle U^{-2}$ is less than 10%, nearly within the measurement uncertainty.

2. Data processing algorithm

The velocity measurements by hot-wire anemometry described in Sec. III A yield the original streamwise velocity signals $\tilde{U}_m(t) = U_m + u_m(t)$ and, consequently, the original time derivative

$$\frac{\partial u_m}{\partial t} \approx \frac{\Delta u_m}{\Delta t} = [u_m(t + f_s^{-1}) - u_m(t)] f_s. \tag{19}$$

It follows that the measured dissipation, estimated from the assumption of isotropic turbulence and Taylor's hypothesis, can be expressed plausibly by

$$\varepsilon_m \approx 15\nu U_m^2 \left\langle(\partial u_m/\partial t)^2\right\rangle \approx 15\nu U_m^2 f_s^2 \left\langle(\Delta u_m)^2\right\rangle. \tag{20}$$

Equation (20) corresponds to the first order two-point backward difference stencil used in numerical simulations. To calculate the derivative more accurately, based on Ref. 45, the present study adopts the algorithm of high-order spectral-like stencils to calculate the velocity gradient (see Ref. 31 for more details).

3. Measurement errors and uncertainties

Experimental uncertainties for the mean velocity (U) and turbulence intensity ($u' = \langle u^2\rangle^{1/2}$), which are those directly measured properties, were inferred directly from estimated inaccuracies in the calibration data and the observed scatter in the results obtained from several repeats of the similar experiment. For the indirectly measured quantities such as the half-radius (R), energy dissipation rate (ε), Taylor length micro-scale (λ), and Kolmogorov length scale (η), the method of propagation of uncertainties was used; those uncertainties resulted from errors in hotwire calibrations and corrections for finite spatial and temporal resolutions of the hotwire probe, etc. A summary of the maximum uncertainty ranges of typical quantities estimated for $x/d = 20$ is given as follows: $[U_c] = \pm 0.5\%$, $[u'] = \pm 1.5\%$, $[\varepsilon] = \pm 8.5\%$, $[\lambda] \approx \pm 3.3\%$, $[\eta] = \pm 3.5\%$, $[\mathrm{Re}_\lambda] = \pm 3.0\%$.

E. Nozzle-exit velocity profiles

To quantify the exit conditions of the jet of investigation, the mean and RMS velocities (U_e, $\langle u_e^2\rangle^{1/2}$) were measured for each of the Reynolds number (Re_d) at $x/d = 0.05$ in the radial direction over the range $-0.6 \le r/d \le 0.6$. Radial profiles of U_e/U_j and $\langle u_e^2\rangle^{1/2}/U_j$ are presented in Figs. 3(a) and 3(b), respectively. A dependence of the exit flow on Re_d is evident. In all cases, approximately top-hat mean exit velocity profiles are produced. However, the extent of uniformity in the varying Re_d profiles differs significantly. As Re_d increases from 4050 to 20 100, the exit profile becomes flatter, and the central region of uniformity widens. A consistent trend of initial turbulence intensity is evident in Fig. 3(b). The peak value of $\langle u_e^2\rangle^{1/2}/U_j$ in the shear layer increases with Re_d, which coincides with the finding of Deo *et al.*[46] for a plane jet. This trend is expected because increasing Re_d must cause a higher instability of the shear layer and thus relatively higher fluctuations of velocity. Moreover, the relative fluctuation intensity across the entire exit plane rises notably with increasing Re_d, despite its value being $\langle u_e^2\rangle^{1/2}/U_j = 0.9\%$-$1.6\%$ over the central region. It should be also noted that the exit flow for each Re_d should be approximately laminar excepting the boundary layer for high Reynolds numbers.

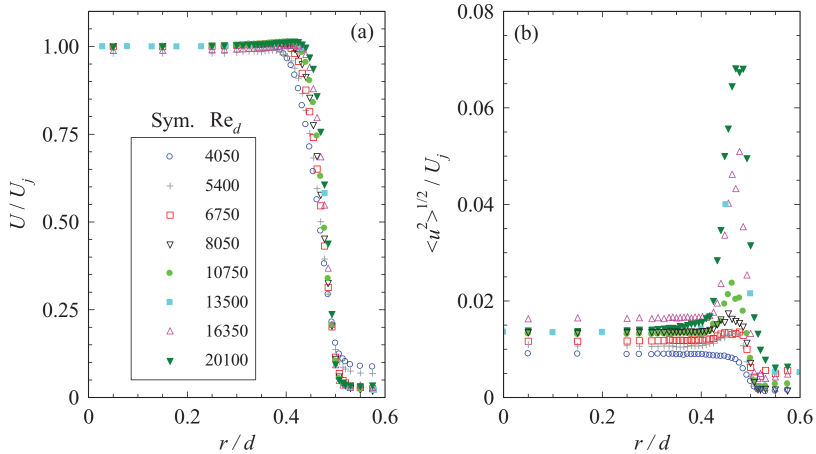

FIG. 3. Inflow conditions at $x/d = 0.05$ for different Re_d. (a) Normalized mean velocity, (b) turbulence intensity.

Figure 4 illustrates the Reynolds-number dependences of the displacement thickness δ and momentum thickness θ of the boundary layer at the jet exit. These thicknesses were calculated from the mean velocity profiles of Fig. 3(a) using the definition equations $\delta = \int_0^\infty (1 - U/U_e)_{x=0.05d}\,dr$ and $\theta = \int_0^\infty U/U_e(1 - U/U_e)_{x=0.05d}\,dr$, respectively. As demonstrated on the plot, both δ and θ decrease appreciably with increasing Re_d from 4050 to 20 100. It is also obvious that the two thicknesses do not become asymptotic over the measured range of Re_d.

The Re_d dependences of U_e/U_j, $\langle u_e^2\rangle^{1/2}/U_j$, δ, and θ observed are expected to transmit downstream to the flow properties and characteristics of the jet. It is important to note that the initial alterations of the mean and RMS velocities and the boundary-layer thicknesses, in general, should not result only from the variation of Re_d but also from that of the nozzle inner geometric profile (e.g., from smooth contraction to sudden contraction or to non-contraction). Nevertheless, given that the present study used a single nozzle of smooth contraction, the exit Reynolds number Re_d should act as the only primary factor for the present case to influence the downstream turbulence properties, which are examined in Secs. IV and V.

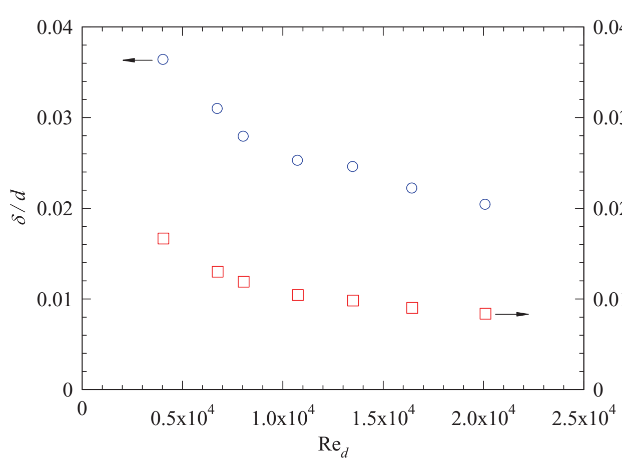

FIG. 4. Reynolds-number dependences of the displacement thickness (δ) and momentum thickness (θ) of the boundary layer at the jet exit.

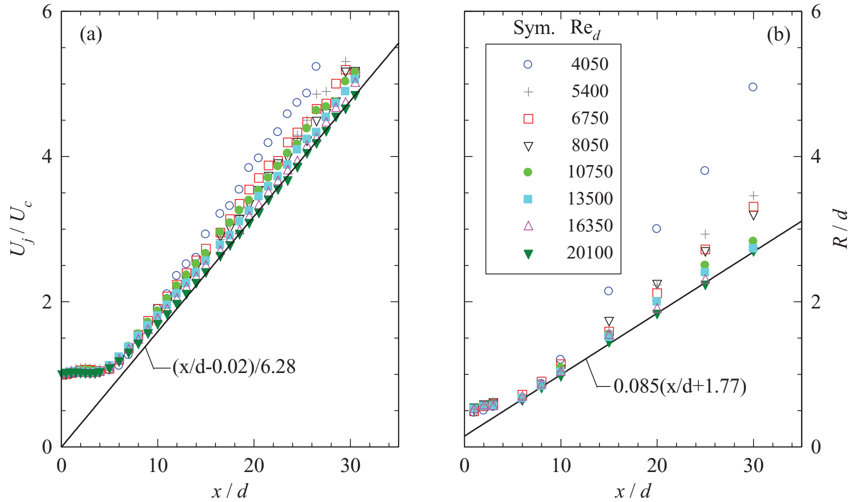

FIG. 5. Streamwise variations of (a) U_j/U_c and (b) R/d for $\mathrm{Re}_d = 4050$–20 100.

IV. REYNOLDS-NUMBER DEPENDENT GLOBAL PROPERTIES

A. Mean velocity decay and spread rates

Figure 5 shows the streamwise variations of the inverse centerline mean velocity U_c normalized by the exit velocity U_j, i.e., U_j/U_c, and the normalized half radius R/d for $4050 \leq \mathrm{Re}_d \leq 20\,100$. In the near field ($x/d < 6$), the Re_d-related variations of U_c and R are quite irregular and within 2.5% and 3.0%, respectively. Farther downstream ($x/d > 6$), the Re_d-dependence becomes regular and significant, see Fig. 5. We access the influence of Re_d on the flow sufficiently downstream using well-known self-preserving relations, i.e., Eqs. (1) and (2). These relations appear to be approximately valid downstream from the potential core including the transition region. Figure 6 demonstrates that the Re_d dependences of U_c and R embodied in K_U and K_R are significant for $\mathrm{Re}_d < 10^4$ but weaken with further increasing Re_d. That is, the present data appear to converge asymptotically at $\mathrm{Re}_d \geq 10^4$

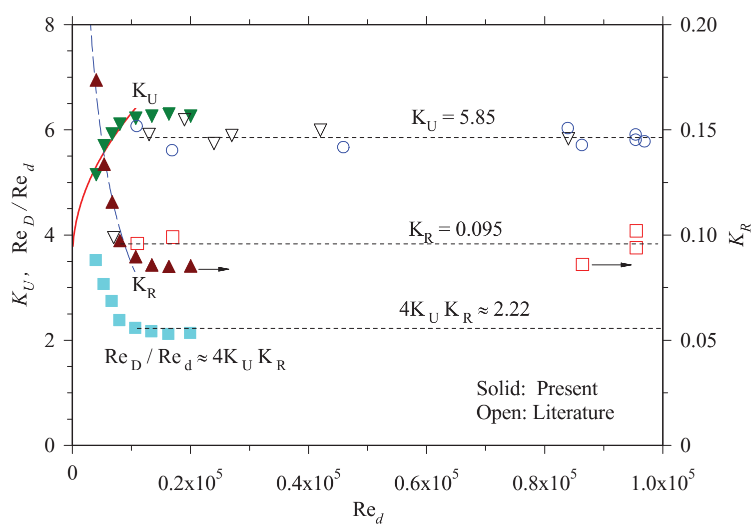

FIG. 6. Dependence on Re_d of the mean velocity decay and spread rates (K_U, K_R) as well as the local Reynolds number $\mathrm{Re}_D = 4U_cR/\nu$. The best-fit curves of the present data for $\mathrm{Re}_d \leq 10^4$: ——, $K_U \approx 0.028\,\mathrm{Re}_d^{1/2} + 3.54$; - - - -, $K_R \approx 14.2\,\mathrm{Re}_d^{-1/2} + 0.055$. Note that the present data are plotted in solid symbols while those from Table I of Ref. 47 are in open symbols.

(note: since the virtual origins are different, the datasets of U_j/U_c and R/d in Fig. 5 for $\mathrm{Re}_d \geq 10^4$ do not collapse on a single curve). Interestingly, a best-fitting suggests that $K_U \approx 0.028\mathrm{Re}_d^{1/2} + 3.54$ and $K_R \approx 14.2\mathrm{Re}_d^{-1/2} - 0.055$ for $\mathrm{Re}_d < 10^4$, both being indicated on the plot. For comparison, also shown in Fig. 5 are some literature data of K_U and K_R obtained from circular jets issuing at high Reynolds numbers from a typical smooth contraction nozzle without any significant flat surface at the exit, which were compiled by Malmström *et al.*[47] (their Table I). The present asymptotic values of K_U and K_R are approximately 6.3 and 0.085, which differ clearly from the averages of the corresponding literature data, which are 5.85 and 0.095 (indicated). Such disparities are believed to result from a different exit configuration of the present nozzle which has a large surface at the exit. Abdel-Rahman *et al.*[48] showed that the effect of an exit wall can reduce the jet entrainment of ambient fluid and thus the centerline velocity decays by about 20%. Taking this into account, the present jets should decay and spread at lower rates, thus corresponding to higher K_U and lower K_R as shown in Fig. 6. In addition, Fig. 6 reveals that a growth in Re_d leads to an increase in K_U and also a decrease in K_R, thus a reduction of jet entrainment in the far field. This agrees with that of Deo *et al.*[46] for a plane jet.

Figure 6 also shows the Re_d dependence of the local Reynolds number defined by the local jet diameter, which is taken commonly as $D = 4R$ (rather than $D = 2R$ which corresponds to the jet central region at $r \leq R$), e.g., see Ref. 24, and the centerline velocity U_c, i.e., $\mathrm{Re}_D = 4U_cR/\nu$. According to the self-preserving relations (1) and (2), it is obtained that $\mathrm{Re}_D/\mathrm{Re}_d \approx 4K_UK_R$. It follows that $\mathrm{Re}_D \approx 2.1\mathrm{Re}_d$ at $\mathrm{Re}_d \geq 10^4$, as seen in Fig. 6. The present asymptotic value of Re_D differs insignificantly from that ($\approx 2.22\mathrm{Re}_d$) estimated from the literature data, suggesting a trivial influence from the flat exit surface of the present nozzle, apparently due to the cancellation of different effects of initial conditions on K_U and K_R.

B. Centerline evolution of the streamwise turbulence intensity

Figure 7(a) shows the streamwise evolution of the normalized centerline turbulence intensity $\langle u^2\rangle^{1/2}/U_c$ at $x/d \leq 30.5$ for different Reynolds numbers. In general, as the jet progresses downstream from the nozzle exit, initially $\langle u^2\rangle^{1/2}/U_c$ increases rapidly, reaches maximum at $x/d \approx 3$–4 and then drops, forming a local peak, which results presumably from the breakdown of primary vortical structures there; farther downstream, the normalized intensity increases again until it asymptotes to a constant for self-preservation. However, it appears from this plot that, in contrast to the mean velocity, the measured variation of $\langle u^2\rangle^{1/2}/U_c$ depends less distinctly on Re_d, especially in the near and transition fields at $x/d < 10$. Yet, a close inspection to the centerline distributions of $\langle u^2\rangle^{1/2}/U_c$ for $x/d \leq 6$ finds that the near-field results exhibit a clear and interesting Re_d-dependent variation: e.g., the peak shifts upstream (and becomes stronger) and then downstream (and weaker) as Re_d is increased. Besides, based on the averaged value of $\langle u^2\rangle^{1/2}/U_c$ over the region $20 \leq x/d \leq 30$, the far-field value of $\langle u^2\rangle^{1/2}/U_c$ denoted by K_I is seen to first decrease with Re_d and then increases asymptotically to $K_I \approx 0.23$ at $Re_d \geq 10^4$, see Fig. 7(b). The establishment of self-preservation for the RMS velocity nevertheless should not be claimed satisfactorily even when the flow has reached the maximum location of the present measurements ($x/d \approx 30$); the similar case has been observed in many previous studies, e.g., Ref. 23.

C. One-dimensional power spectral density of the fluctuating velocity

Dimotakis[2,24] proposed that the mixing transition to the fully developed turbulence manifests itself through a broader spectrum of eddying scales and often marks the beginning of a near $-5/3$ power-law regime, i.e., the Kolmogorov's inertial range, in the energy spectrum with increasing Reynolds number. To inspect this Re_d-dependent aspect, the centerline data of one-dimensional spectrum of the fluctuating velocity (Φ_u) for $x/d \approx 30$ are presented in Fig. 8(a) for eight values of Re_d. Here, Φ_u is defined in $\langle u^2\rangle = \int_0^\infty \Phi_u df$ and f denotes the frequency. It appears that approximately a power-law region, i.e., $\Phi_u \propto f^{-m}$, over a certain range of f approximately occurs in the spectrum approximately for $\mathrm{Re}_d \geq 10^4$, carefully see Fig. 8(b); also, the range span widens as Re_d increases.

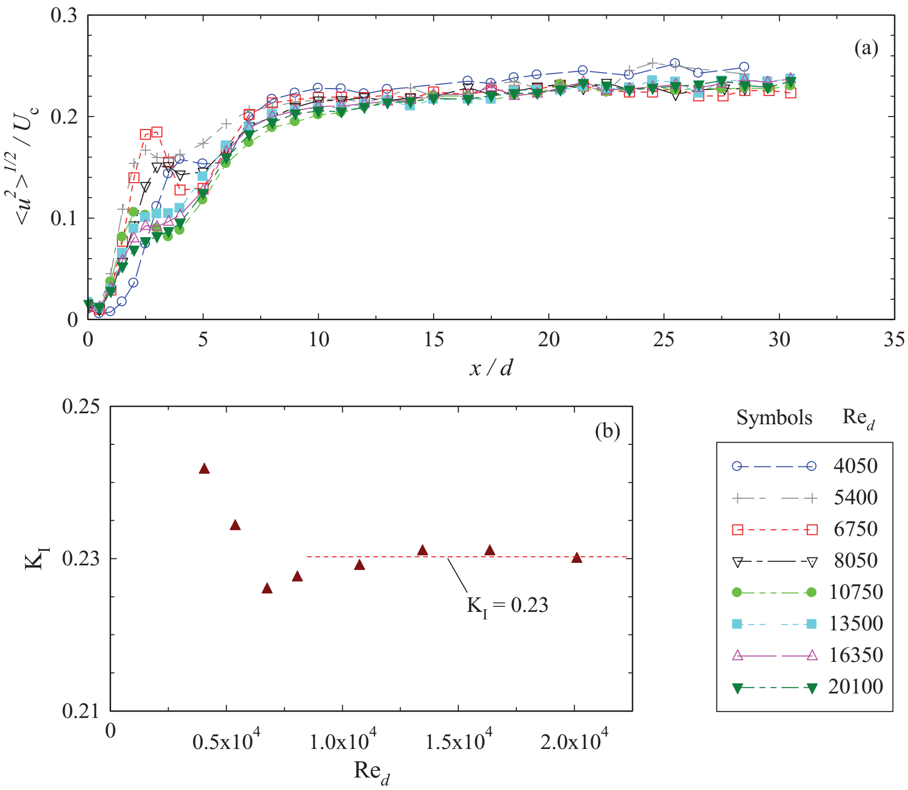

FIG. 7. (a) Normalized streamwise RMS velocity distribution ($\langle u^2 \rangle^{1/2}/U_c$) along the centerline and (b) Re_d dependence of the averaged value of K_I over the range $20 \leq x/d \leq 30$.

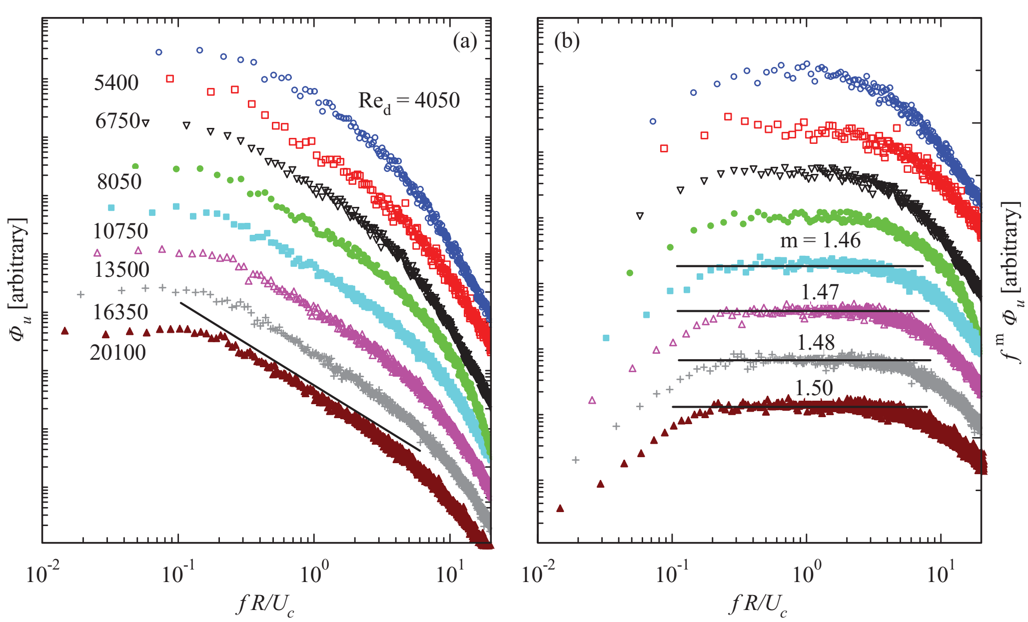

FIG. 8. Reynolds number dependent spectra of the centerline u measured at $x/d = 30$. (a) $\Phi_u^*(f)$; (b) $f^m \Phi_u^*(f)$. Note that the spectra were corrected for the effects of finite hotwire length and measurement sampling rate.

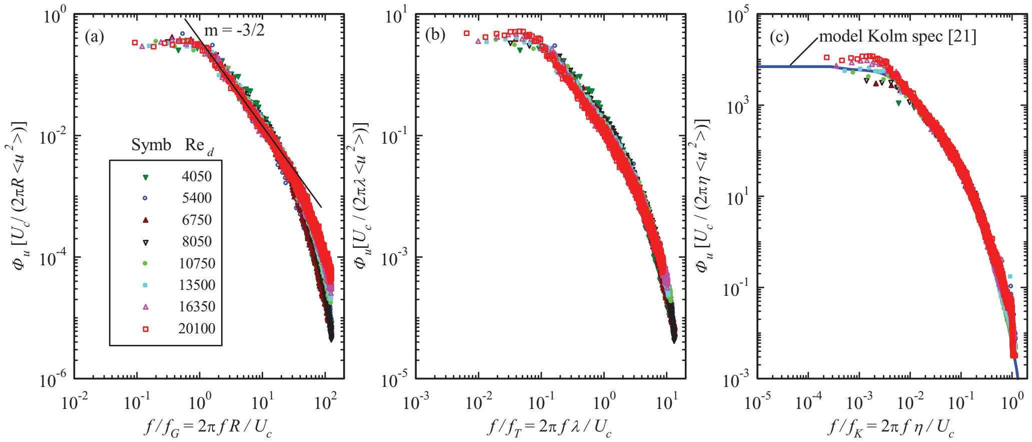

FIG. 9. Reynolds number dependent spectra of the centerline u measured at $x/d = 30$. (a) $\Phi_u(f)[U_c/(2\pi R\langle u^2\rangle)]$ vs. $2\pi fR/U_c$; (b) $\Phi_u(f)[U_c/(2\pi\lambda\langle u^2\rangle)]$ vs. $2\pi f\lambda/U_c$; (c) $\Phi_u(f)[U_c/(2\pi\eta\langle u^2\rangle)]$ vs. $2\pi f\eta/U_c$, with a model Kolmogorov spectrum for $\mathrm{Re}_\lambda = 130$ from Pope.[21] Note that the spectra were corrected for the effects of finite hotwire length and sampling rate.

However, the power-law exponent (m) is not 5/3, the famous exponent of Kolmogorov, derived by assuming local isotropy, and instead $m \leq 1.5$. To confirm this more convincingly, the compensated spectra $f^m\Phi_u$ for $m = 1.46$–1.5 are shown in Fig. 8(b), which indeed enhances the observation. Although the increase in m is small due to a narrow variation in Re_d from 10 750 to 20 100, the result is consistent with, e.g., the previous observation for grid turbulence.[49] It has been generally accepted that, as Reynolds number increases, m increases gradually and approaches 5/3 asymptotically. Note nevertheless that the value of $m \approx 1.5$ was observed by Mi and Antonia[50] and Burattini *et al.*[51] for a circular jet at two very different values of $\mathrm{Re}_d \approx 16\,000$ and 130 000, respectively. This suggests that the centerline value of m is highly insensitive to the magnitude of Re_d. Of note, also, Mi and Antonia[50] found that m increases as the large-scale intermittency factor γ (the fraction of time when turbulence occurs) decreases, so that the value of $m = 5/3$ is achieved at a radial location far away from the centerline where $\gamma < 1$ (partially turbulence), compared with constantly turbulence on the centerline where $\gamma = 1$. It is hence suggested that the existence of a power-law range represents the presence of the inertial range of turbulence no matter whether $m = 5/3$ or not.

Figures 9(a)–9(c) display the Φ_u distributions normalized, respectively, by R, λ, and η to inspect the Re_d dependence of Φ_u under the global-scale (R), inertial-scale (λ), and dissipative-scale (η) normalizations. Here, it is assumed that the Kolmogorov frequency $f_K = U_c/2\pi\eta$, the Taylor-scale frequency $f_T = U_c/2\pi\lambda$, and the global characteristic frequency $f_G = U_c/2\pi R$. Apparently, all the data sets collapse very well at $2\pi fR/U_c < 20$ for $\mathrm{Re}_d = 8050$–$20\,100$, Fig. 9(a), by the global-scale normalization and at $2\pi f\eta/U_c \geq 0.01$ for all Re_d, Fig. 9(c), by the dissipative-scale normalization. Of note, the data given in Fig. 9(c) are normalized by the Kolmogorov scales, which appear to compare perfectly well at $2\pi f\eta/U_c \geq 0.01$ with the model Kolmogorov spectrum for $\mathrm{Re}_\lambda = 130$ presented in Fig. 6.14 of Pope,[21] despite $m = 5/3$ for the latter. When λ is used for normalization, the normalized distributions collapse quite well over the entire range of f for $\mathrm{Re}_d = 8050$–$20\,100$, Fig. 9(b), similar to the result of Burattini *et al.*[51] for different initial conditions.

V. REYNOLDS-NUMBER DEPENDENT SMALL-SCALE PROPERTIES

A. Checks to the appropriateness of the corrected dissipation measurements

As described in Sec. III, the total dissipation rate ε was presently measured from the streamwise component $\varepsilon_{xx} = 5\nu\langle(\partial u/\partial x)^2\rangle$ by assuming local isotropy, i.e., $\varepsilon \approx 3\varepsilon_{xx} = 15\nu\langle(\partial u/\partial x)^2\rangle$. Here, using the case of $\mathrm{Re}_d = 20\,100$, for which the largest correction for the hotwire length is needed, an indirect check to the appropriateness of the dissipation measurements is made along the centerline

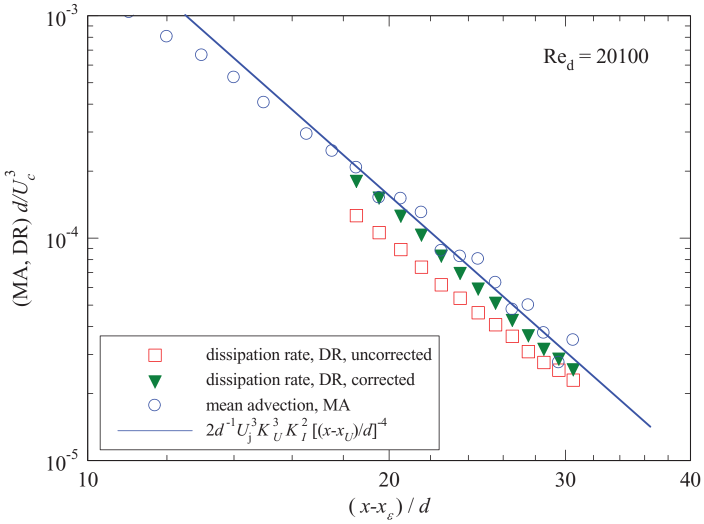

FIG. 10. Centerline evolutions of two axial budget terms of the turbulent kinetic energy: the mean advection (MA), $-U_c\partial\langle u^2\rangle/\partial x$, and the dissipation rate (DR), $-2\varepsilon_{xx}$, at Re$_d$ = 20 100. Note that the dissipation data were corrected for the effects of finite hotwire length and sampling rate.

through the assessment of the axial budget of the kinetic energy, which can be expressed as[19,20]

$$0 = -U_c\frac{\partial\langle u^2\rangle}{\partial x} - \frac{2}{\rho}\left\langle u\frac{\partial p}{\partial x}\right\rangle - \left[\frac{\partial\langle u^3\rangle}{\partial x} + \frac{1}{r}\frac{\partial(r\langle vu^2\rangle)}{\partial r}\right] - 2\langle u^2\rangle\frac{\partial U_c}{\partial x} - 2\varepsilon_{xx}. \tag{21}$$

In Eq. (21), on the right-hand side, the first term is for the mean advection (MA), the second for the pressure work (PW), the third for the turbulence transport (TT), the fourth for the turbulence production (TP), and the fifth for the DR, all being the axial components. Based on Eqs. (1) and (3) for U_c and $\langle u^2\rangle$, it is obtained that

$$\mathrm{TP} = \mathrm{MA} = 2d^{-1}U_j^3K_U^3K_I^2\left(\frac{x-x_U}{d}\right)^{-4}, \tag{22}$$

which indicates that the mean advection is equal to the turbulence production along the centerline in the self-preserving region. Figure 10 illustrates the centerline evolutions of two axial budget terms of Eq. (21): i.e., the normalized MA, $-(U_c\partial\langle u^2\rangle/\partial x)(U_j^{-3}d)$, and the normalized DR, $2\varepsilon_{xx}(U_j^{-3}d)$, at Re$_d$ = 20 100. Note that both the corrected and uncorrected values for DR are presented on the plot. Evidently, the present measurements show that the corrected $2\varepsilon_{xx}$ is only slightly ($\sim$10%) smaller than $-U_c\partial\langle u^2\rangle/\partial x$. This is consistent with the previous measurements of Panchapakesan and Lumley[19] and Hussein *et al.*[20] in a similar jet but under different initial and boundary conditions. Lipari and Stansby[52] summarized in their review that on the centerline $2\varepsilon_{xx} \approx -0.97U_c\partial\langle u^2\rangle/\partial x$ and $-0.99U_c\partial\langle u^2\rangle/\partial x$, respectively, from Refs. 19 and 20. These authors further claimed that "both sets of centerline values follow the same structure $\mathrm{MA_c} \equiv \mathrm{TP_c} \approx |2\varepsilon_{xx}|_c = |\mathrm{TT_c} - \mathrm{PW_c}|$, irrespective of the different approaches to modeling dissipation." (Here, the subscript "c" means "on-centerline.") Suppose that the approximation $\mathrm{MA_c} \approx |2\varepsilon_{xx}|_c$ is valid and also that the previously measured dissipations are adequate. Then, the present measurements of $|2\varepsilon_{xx}|_c$ should be considered appropriate since the present MA$_c$ was obtained as properly as those in the previous studies.[19,20] Moreover, Fig. 10 shows that Eq. (22) works quite well for $(x-x_\varepsilon)/d \geq 18$ while MA$_c$ exhibits a slower streamwise decay rate than that obtained from Eq. (22) at $(x-x_\varepsilon)/d < 18$. The invalidity of Eq. (22) in the transition region is expected from the fact that the self-preservation of $\langle u^2\rangle$ there is yet to be developed, i.e., $\langle u^2\rangle^{1/2}/U_c \neq$ constant (see Fig. 7(a)). In addition, the effectiveness of the correction described in Sec. III B is illustrated in Fig. 10. Clearly, the difference between the corrected and uncorrected $|2\varepsilon_{xx}|_c$ decreases with downstream distance x. This can be well explained here: as x increases, the Kolmogorov scale η increases, so the relative hotwire length l_w/η decreases, and

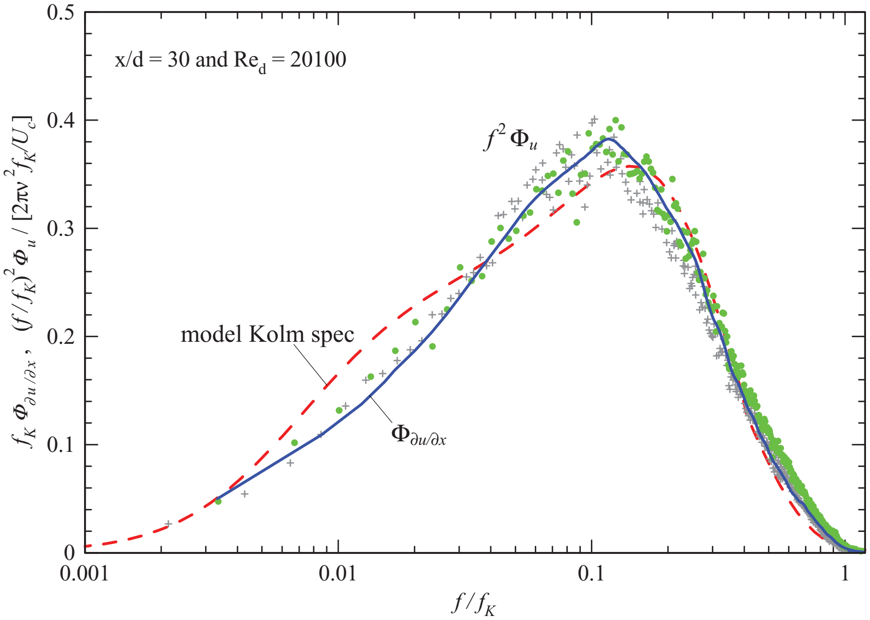

FIG. 11. Normalized on-centerline spectrum of u weighted by f^2 (●, +) and that of $\partial u/\partial x$ (—, smoothed) obtained at $x/d = 30$ for $\mathrm{Re}_d = 20\,100$ or $\mathrm{Re}_\lambda \approx 130$ with the model Kolmogorov spectrum (- - - -) for $\mathrm{Re}_\lambda = 130$ from Pope.[21] Note that the data denoted by + were not corrected for the effects of hotwire length and sampling rate.

hence the spatial contamination reduces. As expected, the uncorrected $|2\varepsilon_{xx}|_c$ data do not follow the power-law x^{-4}.

Also, the appropriateness of the dissipation measurements may be checked by comparing the Kolmogorov-normalized spectrum of u weighted by f^2 and that of $\partial u/\partial x$, i.e., $(f/f_K)^2\,\Phi_u[U_c/(2\pi\nu^2 fK)]$ and $f_K\,\Phi_{\partial u/\partial x}$, with the model Kolmogorov spectrum. The comparisons are made in Fig. 11, which presents the current spectra obtained on the centerline at $x/d = 30$ for $\mathrm{Re}_d = 20\,100$ or $\mathrm{Re}_\lambda \approx 130$ and the model spectrum produced from Fig. 6.14 of Pope[21] for $\mathrm{Re}_\lambda = 130$. Pope[21] claims that the model spectrum is generally quite accurate at $k_1\eta = f/f_K > 0.1$. In other words, the spectrum should be fairly trustworthy at high frequencies, i.e., not affected by noise and spatial resolution, from which the correctness of the measured spectra can be verified. Indeed, Fig. 11 demonstrates that the present measurements agree well (within 10%) with the model spectrum for $k_1\eta \geq 0.2$. This provides an indirect support for the appropriateness of the present estimates of the measured dissipation using the digital filter of Mi *et al.*[30,31] to remove high-frequency noises and the correction approach of Antonia and Mi[40] for the limited wire length and sampling rate. The considerable difference observed between the measured data and the model spectrum for $k_1\eta \leq 0.15$ reflects the difference noted above that the present inertial-range exponent of the velocity spectrum is $m \approx 1.5$ versus $m = 5/3$ or 1.67 for the model spectrum.[21] In addition, it is interesting to note that the distributions of $f^2\Phi_u$ and $\Phi_{\partial u/\partial x}$ are highly consistent with each other. This consistence might derive from two causes: (1) the approximately valid assumption of local isotropy that enables $\int_0^\infty \Phi_{\partial u/\partial x}(f)df = \int_0^\infty f^2\Phi_u(f)df$ and (2) the close connection of the two spectra due to the present use of $\partial u/\partial x \approx -U^{-1}\partial u/\partial t$ for $\Phi_{\partial u/\partial x}$. On the other hand, such a good consistence of $f^2\Phi_u$ and $\Phi_{\partial u/\partial x}$ may provide more evidence, though indirect, to further support for the appropriateness of the present dissipation measurements.

B. Dissipation rate and Kolmogorov length scale

Figure 12 presents the streamwise evolution of the normalized dissipation rate $\varepsilon^* = \varepsilon d/U_j^3$ for $\mathrm{Re}_d = 4050$–$20\,100$. As the jet develops downstream, ε^* decreases rapidly with downstream distance

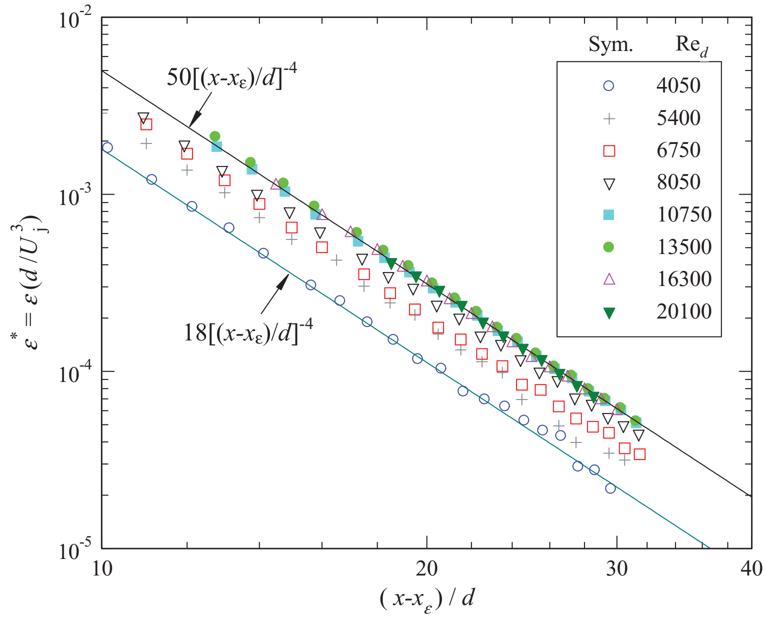

FIG. 12. Streamwise evolution of the normalized energy dissipation rate $\varepsilon^* = \varepsilon\,(U_j^{-3}d)$. Note that the dissipation data have been corrected for the effects of finite hotwire length and sampling rate.

x; this decrease follows Eq. (6) well for all $x \geq x_A$ or based on all the post-filtering data (see Fig. 2). However, the region where Eq. (6) is valid should not be only limited for $x \geq x_A$. Figure 12 shows that the validity occurs at $x/d \geq 10$ for the lowest $\mathrm{Re}_d = 4050$ while an increase in Re_d is expected to widen the valid region for Eq. (6). It follows that the self-preserving state of ε should be established at least at $x/d \geq 10$ for all the measured values of $\mathrm{Re}_d \geq 4050$. For $\mathrm{Re}_d \leq 10^4$, as observed from Fig. 13, the prefactor (C_ε) of Eq. (6) increases with Re_d. For $\mathrm{Re}_d > 10^4$, nevertheless, all the measured data of ε^* becomes constant and collapses virtually onto a single horizontal line with $C_\varepsilon \approx 50$, suggesting that ε^* becomes nearly independent of the Reynolds number. This value of C_ε agrees closely with $C_\varepsilon = 48$ obtained by Friehe *et al.*[36] for $\mathrm{Re}_d = 1.2 \times 10^5$, and was also verified later by Antonia *et al.*[25] for circular jets at three different Reynolds numbers $\mathrm{Re}_d = 5.56 \times 10^4$, 1.09×10^5, and 4.71×10^5.

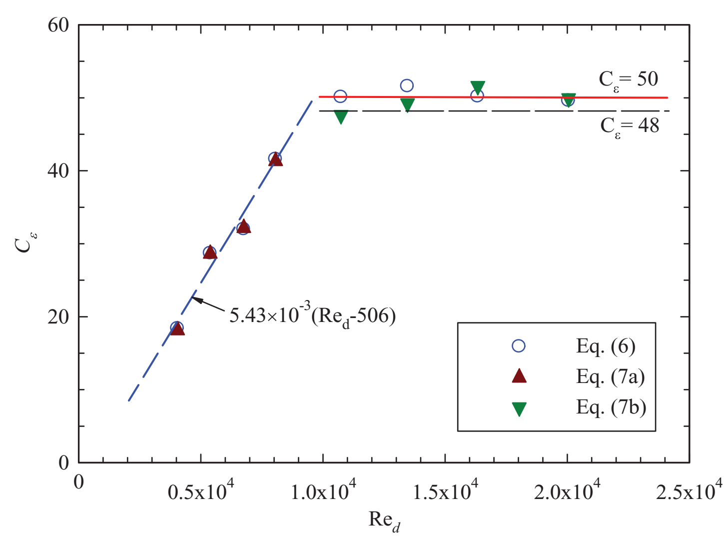

FIG. 13. Dependence on Re_d of the prefactor C_ε of Eq. (6).

Figure 13 illustrates, more clearly, the dependence of C_ε on Re_d estimated from Eqs. (6)–(7b). These estimations are in good agreement, within experimental uncertainties. It is therefore evident that all Eqs. (6)–(7b) work very well in the circular jet at least for $\mathrm{Re}_d \geq 4050$. In addition, it is interesting to note from Fig. 13 that C_ε increases approximately linearly with Re_d, i.e., $C_\varepsilon \propto \mathrm{Re}_d$, at $\mathrm{Re}_d \leq 10^4$. This seems at variance with Eq. (7a): $C_{\varepsilon l} = K_{\varepsilon l} K_U^2 K_R^{-2} \mathrm{Re}_d^{-1}$. However, see Fig. 6, for $\mathrm{Re}_d \leq 10^4$, both K_U and K_R are correlated with Re_d as $K_U \sim \mathrm{Re}_d^{1/2}$ and $K_R \sim \mathrm{Re}_d^{-1/2}$ and, consequently, $C_{\varepsilon l} \approx 5.43 \times 10^{-3}$ ($\mathrm{Re}_d - 506$), as indicated on the plot. In summary, Fig. 13 suggests that, as the Reynolds number grows from the lowest value (4050), C_ε increases approximately linearly from 20 to 50 at $\mathrm{Re}_d \leq 10^4$ and becomes nearly constant for $\mathrm{Re}_d > 10^4$.

Substituting $C_\varepsilon \approx 50$ into Eq. (7b), we obtain $K_{\varepsilon h} \approx 0.017$ for $\mathrm{Re}_d \geq 10^4$, while Antonia *et al.*[25] obtained the constant of 0.029 with $K_U \approx 5.4$, $K_R \approx 0.1$ at $\mathrm{Re}_d = 4.71 \times 10^5$. For the case of $\mathrm{Re}_d < 10^4$, C_ε reduces with decreasing Re_d. The constant $K_{\varepsilon l}$ can be obtained by substituting C_ε into Eq. (7a). The result is that $K_{\varepsilon l} = 83.5$, 82.7, 82.1, and 83.1 for $\mathrm{Re}_d = 4050$, 5400, 6750, and 8050, respectively. Here, we take the average of the four values of $K_{\varepsilon l}$ as the constant in Eq. (4), i.e., $K_{\varepsilon l} \approx 83$. To our best knowledge, no previous systematic studies have been performed to obtain $K_{\varepsilon l}$ for $\mathrm{Re}_d < 10^4$. In other words, we are likely to have made the first estimation of $K_{\varepsilon l}$ for any turbulent flow, even though presently invoking the isotropic assumption and Taylor's hypothesis. Hence, in the self-preserving far field of the circular SC jet, the typical centerline dissipation rate may be estimated roughly from $\varepsilon \approx 83\nu U_c^2/R^2$ for $\mathrm{Re}_d < 10^4$.

Figure 14 shows the centerline evolution of the normalized Kolmogorov length scale η/d for $\mathrm{Re}_d = 4050$–20 100. Evidently, η increases linearly with x for each value of Re_d, thus validating Eq. (8) or $\eta/d = C_\eta\,[(x - x_\eta)/d]$. Figure 14 also demonstrates that η decreases with increasing Re_d. To inspect the Re_d dependence of η/d in more detail, the measured data of η/d is substituted to Eq. (8) to obtain C_η directly. The results are presented in Fig. 15. For high Reynolds numbers at $\mathrm{Re}_d \geq 10^4$, C_η is proportional to $\mathrm{Re}_d^{-3/4}$ and can be expressed as $C_\eta = 50^{-1/4}\mathrm{Re}_d^{-3/4} \approx 0.37\mathrm{Re}_d^{-3/4}$. It follows that

$$\eta/d \approx 0.37\mathrm{Re}_d^{-3/4}(x - x_\eta)/d \tag{23}$$

for $\mathrm{Re}_d \geq 10^4$. Interestingly, Eq. (23) is nearly the same as that obtained from Antonia *et al.*[25] and also from Eq. (22) of Dimotakis[24] together with his local jet diameter $D = 4R \propto 0.4x$. Considering very different experimental setups and laboratory conditions used by the present and previous studies, this agreement appears to imply that the variation of Kolmogorov scale is weakly dependent on (or insensitive to) the initial and boundary conditions. By comparison, Fellouah and Pollard[27] reported a much smaller prefactor ($160^{1/4} \approx 0.28$) of Eq. (23); they attributed the significant difference

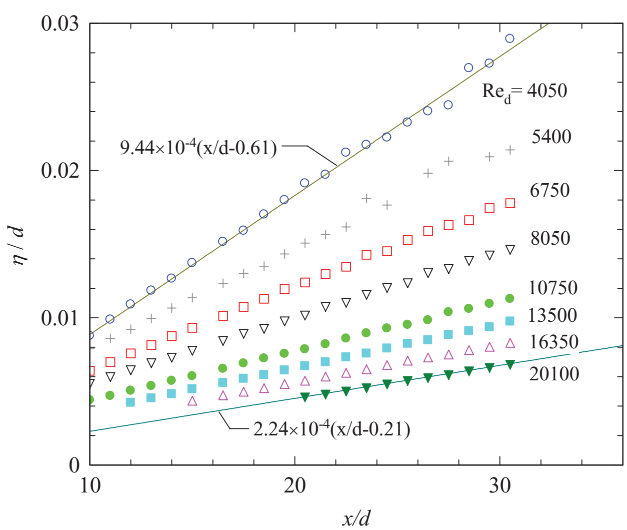

FIG. 14. Streamwise evolution of normalized Kolmogorov length scale η/d for $\mathrm{Re}_d = 4050$–20 100.

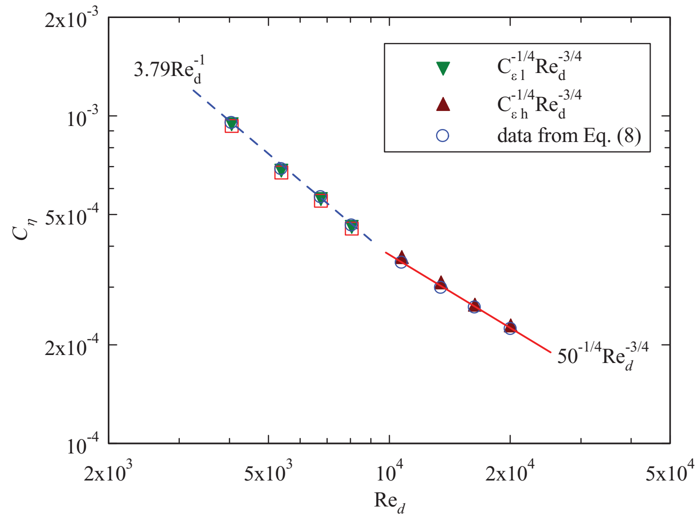

FIG. 15. Dependence of C_η on Re_d.

of about 30% to their application of a flying hotwire (no need of Taylor's hypothesis) relative to that of a stationary hotwire by Antonia *et al.*[25] which requires the use of Taylor's hypothesis. This is however unexpected because, as shown by Mi and Antonia,[42] the error caused by the hypothesis is less than 10% along the jet centerline. It is anticipated that the lower prefactor resulted mainly from their data being significantly contaminated by the high-frequency noise. Note that their fluctuating velocity signals were improperly filtered at a very high frequency (15 kHz), consequently well underestimating λ and η since the velocity time derivative and thus the dissipation rate were overestimated, see Ref. 31.

To compare η with D (=4R), the manipulation of Eqs. (2) and (21) obtains that

$$\eta/D \approx 1.1\mathrm{Re}_d^{-3/4} \tag{24}$$

for $\mathrm{Re}_d \geq 10^4$, presently with $K_R = 0.085$ and assuming that $x_\eta = x_R$. The ratio η/D is somewhat different from that obtained by Dimotakis,[24] which is $\eta/D \approx 0.95\mathrm{Re}_d^{-3/4}$; this is reflected in the prefactor (1.12 versus 0.95). Some explanation follows. As noted earlier, the exit surface of the present nozzle weakened the jet's entrainment and the spreading rate, thus decreasing D, but imposed little influence on η. In this context, there is a point to make here: the presence of the exit surface or generally the inlet condition affects the far-field global characteristics but not fine-scale turbulence of the jet.

For lower Reynolds numbers at $\mathrm{Re}_d < 10^4$, Fig. 15 suggests that the prefactor C_η can be obtained by $C_\eta = C_{\varepsilon l}^{1/4}\mathrm{Re}_d^{-3/4} \approx 3.8\mathrm{Re}_d^{-1}$, which agrees very well with that from the measured data of Fig. 14. It follows that, for $\mathrm{Re}_d < 10^4$, the magnitudes of the Kolmogorov scale η relative to the jet exit and local diameters (d, D) can be approximated by

$$\eta/d \approx 3.8\mathrm{Re}_d^{-1}(x - x_\eta)/d \tag{25}$$

and

$$\eta/D \approx 0.065\mathrm{Re}_d^{-1/2}, \tag{26}$$

respectively, which differ considerably from those, i.e., (23) and (24), for high Reynolds numbers.

C. Taylor length scale and turbulent Reynolds number

Figure 16 shows the normalized Taylor length scale λ/d along the centerline for $\mathrm{Re}_d = 4050$–20 100. Like η/d (see Fig. 13), the centerline λ/d also increases linearly with downstream distance, thus proving Eq. (9). It is also evident that λ decreases as the Reynolds number is increased. To

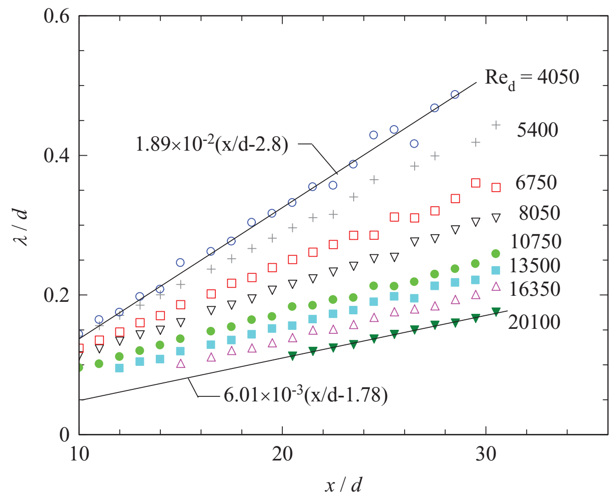

FIG. 16. Streamwise evolution of normalized Taylor length scale λ/d for $\mathrm{Re}_d = 4050$–20 100.

further examine the effect of Re_d on λ, Fig. 16 displays the results of C_λ estimated from the λ/d data via Eq. (9). For $\mathrm{Re}_d < 10^4$, C_λ decreases inversely linearly with the Reynolds number, with $C_\lambda \mathrm{Re}_d \approx 75.4$. In other words, for the present jet at $\mathrm{Re}_d < 10^4$, the ratios λ/d and λ/D can be obtained by

$$\lambda/d \approx 75.4\mathrm{Re}_d^{-1}(x - x_\lambda)/d, \tag{27}$$

$$\lambda/D \approx 1.25\mathrm{Re}_d^{-1/2}. \tag{28}$$

It is also deduced from Figure 17 that, for $\mathrm{Re}_d \geq 10^4$, C_λ is proportional to $\mathrm{Re}_d^{-1/2}$ so that $C_\lambda \mathrm{Re}_d^{1/2} \approx 0.82$. Therefore, for the present jet of high Reynolds numbers, the ratios λ/d and λ/D are different from Eqs. (27) and (28) and can be expressed as

$$\lambda/d \approx 0.82\mathrm{Re}_d^{-1/2}(x - x_\lambda)/d, \tag{29}$$

$$\lambda/D \approx 2.41\mathrm{Re}_d^{-1/2}. \tag{30}$$

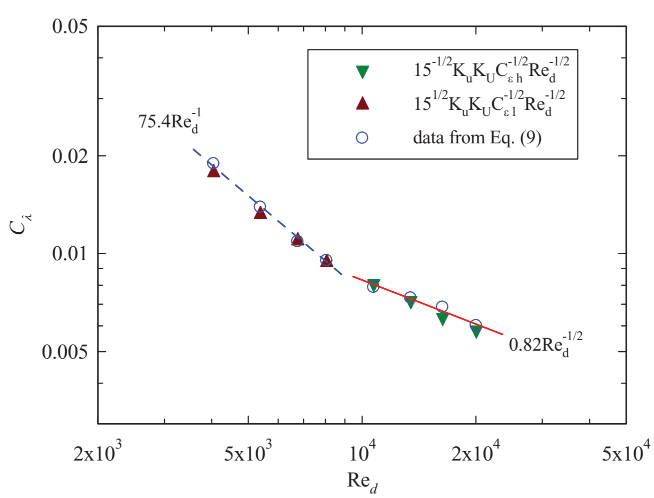

FIG. 17. Dependence of C_λ on Re_d.

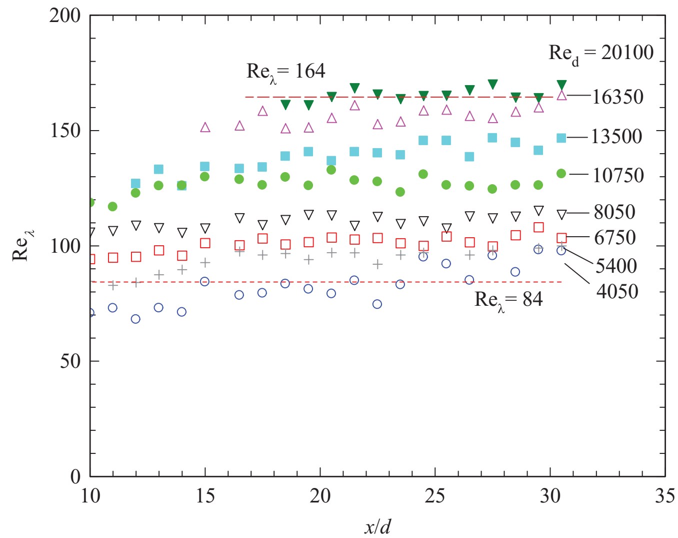

FIG. 18. Centerline evolution of turbulent Reynolds number Re_λ for $Re_d = 4050$–20 100.

Note that the prefactor of Eq. (29) is slightly smaller than that (=0.88) obtained by Antonia *et al.*[25] while that of Eq. (30) is bigger than that (=2.3) of Dimotakis.[24] These differences, and also those associated with η, are likely due mainly to the discrepancies in nozzle exit geometry (the point has been made earlier). Again, as expected, the prefactor (0.79) of Eq. (29) from Fellouah and Pollard[27] was rather underestimated, highly likely due to an improper filtering of the high-frequency noise from the velocity signals.

Figure 18 presents the centerline evolution of Re_λ (turbulent Reynolds number) for $\mathrm{Re}_d =$ 4050–20 100. Apparently, Re_λ is nearly constant along the centerline of the circular jet for any given value of Re_d, even though the scattering of each data set is obvious. Note that this evident scatter results mainly from the ratio $K_I = u'/U_c$ (see Fig. 7). Taking the average of Re_λ for $x/d \geq 20$, the mean values of Re_λ were obtained and are plotted against Re_d in Fig. 19. Apparently, for $\mathrm{Re}_d > 10^4$, the relationship of Re_λ with Re_d can be expressed approximately as (indicated on the plot)

$$\mathrm{Re}_\lambda \approx 1.16\mathrm{Re}_d^{1/2}, \tag{31}$$

where the prefactor (1.16) is smaller than that (1.74) obtained from Antonia *et al.*[25] and greater than that (1.04) from Champagne[44] for $\mathrm{Re}_d = 3.7 \times 10^5$. Nevertheless, the data from the two previous studies were obtained only at one or three high Reynolds numbers, compared with ours from five values of Re_d. Dimotakis[24] and his co-workers (e.g., Ref. 53) obtained that $\mathrm{Re}_\lambda \approx 1.4\mathrm{Re}_d^{1/2}$, based on the measurements in the jets issuing from a conventional smooth-contraction nozzle (without a large exit surface). In addition, to compare the Re_D–Re_d and Re_λ–Re_d relationships, the dependence of Re_D on Re_d is also shown in Fig. 19; it is well proven that $\mathrm{Re}_D \approx 2.1\mathrm{Re}_d$ at $\mathrm{Re}_d \geq 10^4$.

Although the present results of η/d and λ/d are nearly identical to those of Antonia *et al.*,[25] there are relatively large discrepancies between the two investigations with respect to Re_λ. This is mainly due to the measurement differences in the turbulence intensity $K_I = \langle u^2\rangle^{1/2}/U_c$, which might result from different initial and boundary conditions. On the other hand, this implies that behaviors of the smallest-scale turbulence are more universal or depend less on the flow configuration or initial and boundary conditions.

D. Comparison of virtual origin locations x_U, x_R, x_ϵ, x_λ, and x_η

When a turbulent flow has reached the self-preserving state, ideally, the self-preservation is expected to apply for all different scales from the smallest to the largest in the flow. Hence, the five virtual origin locations associated with Eqs. (1), (2), (6), (8), and (9) are expected to be identical,

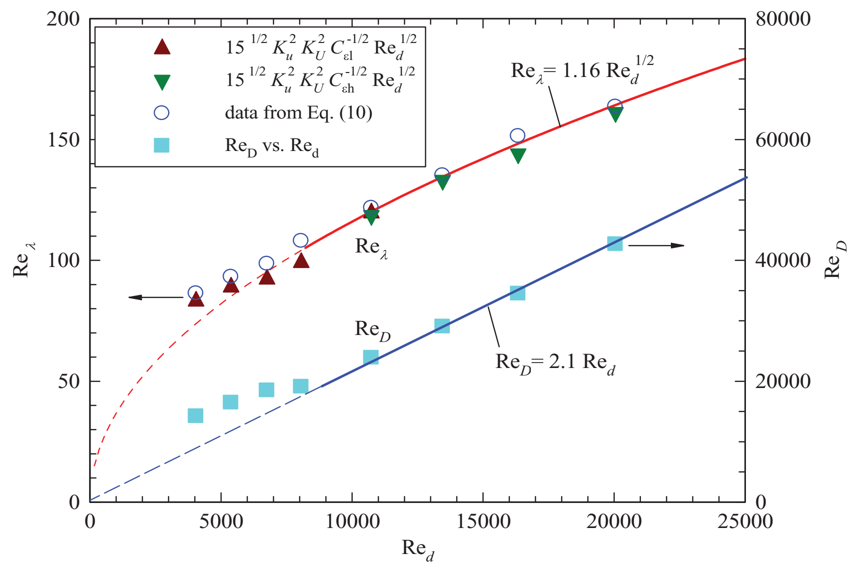

FIG. 19. Dependence of Re_λ and Re_D on Re_d.

i.e., $x_U = x_R = x_\varepsilon = x_\lambda = x_\eta$, according to the traditional assumption (e.g., Hinze[37] and Chen and Rodi[54]). However, Fig. 20 demonstrated that these virtual origin locations differ appreciably and that the resulting differences should not derive just from the measurement inaccuracy. This observation is consistent with the previous work (e.g., Ref. 55) that x_U is often different from x_R, even both being for the mean flow. In this context, we anticipate that all the five locations are truly distinct. Moreover, Fig. 20 reveals that, as Re_d increases, all the virtual origins initially move upstream, reach their minimum values, and then turn to shift downstream. Consistent with the above observations, all the minima appear to occur at $\mathrm{Re}_d \approx 10^4$.

E. Skewness and flatness factors of $\partial u/\partial x$

Figures 21 and 22 show, respectively, the skewness and flatness factors (S, F) of the longitudinal velocity derivative $\partial u/\partial x$ versus the Taylor Reynolds number Re_λ, where the two factors are defined

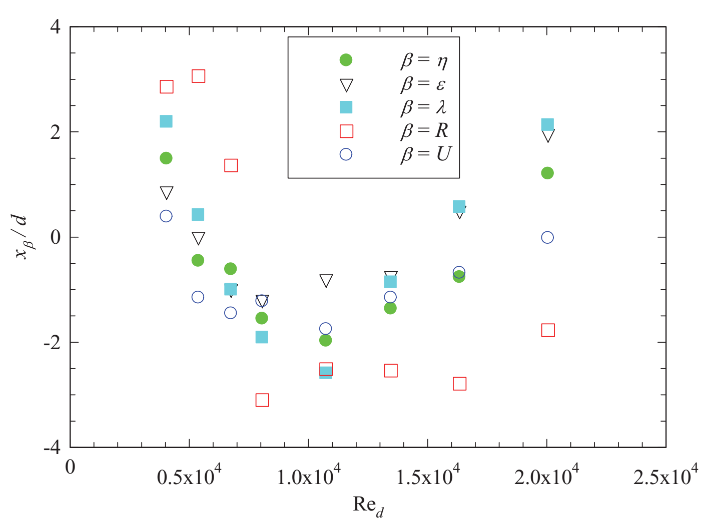

FIG. 20. Different virtual origin x-locations versus Re_d.

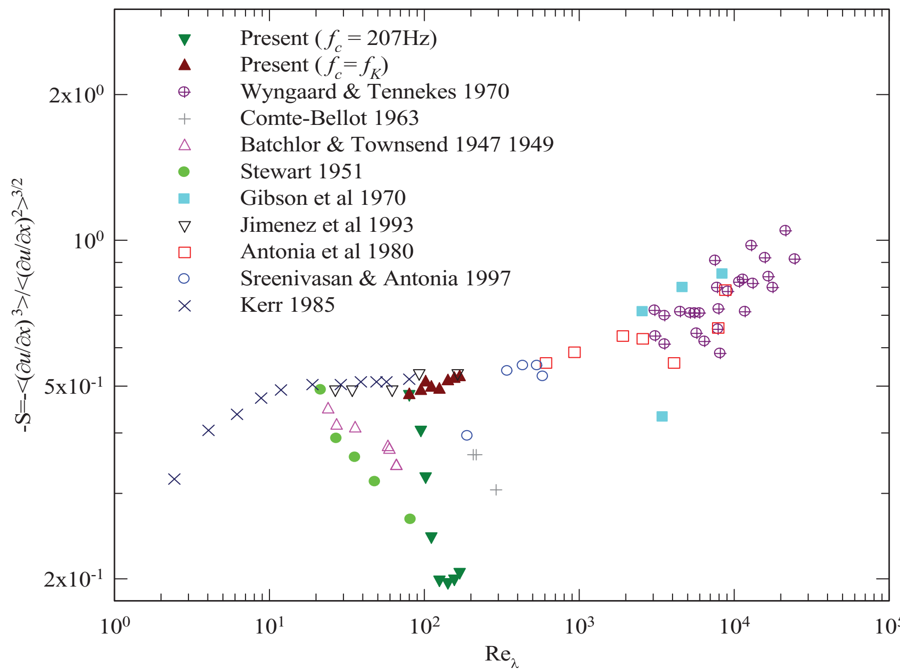

FIG. 21. Re_λ dependence of the skewness factor of $\partial u/\partial x$ for various turbulent flows. Present data were obtained at $x/d = 25$ in a circular jet. All the literature data were compiled in Ref. 1.

by $S \equiv \langle(\partial u/\partial x)^3\rangle\langle(\partial u/\partial x)^2\rangle^{-3/2}$ and $F \equiv \langle(\partial u/\partial x)^4\rangle\langle(\partial u/\partial x)^2\rangle^{-2}$. For comparison, all the data compiled in Ref. 1 for various turbulent flows are also displayed. Apparently, the present data for both factors match well with those obtained previously for different flows. In the present range of $Re_\lambda \approx 80$–170, both S and F generally increase with increasing Re_λ. This can be extended to the whole range of Re_λ when considering previous investigations in the atmosphere, in laboratory flows,

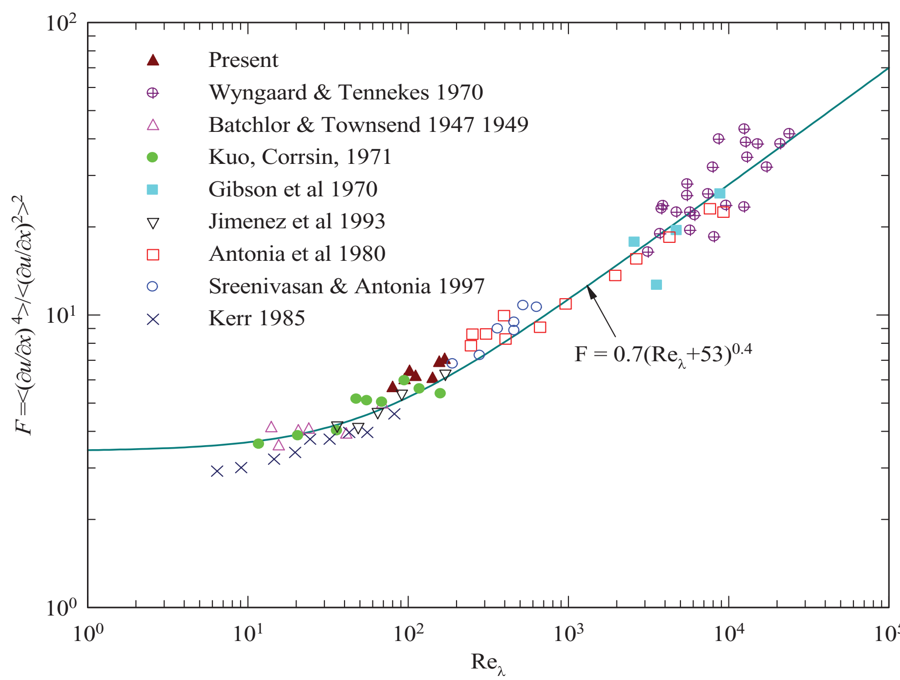

FIG. 22. Dependence on Re_λ of the flatness factor of $\partial u/\partial x$ for various turbulent flows. Present data were obtained at $x/d = 25$ in a circular jet. All the literature data were compiled in Ref. 1.

and from numerical simulations. Such an observation is obviously at variance with the hypothesis of Kolmogorov[33] or K41 for short, in which both the skewness and flatness factors of velocity derivatives are assumed to be constant and independent of Reynolds number. This suggests that K41 be an over-simplified model and cannot be regarded as universal.[1]

Significantly, unlike the quantities reported above, the variations of both factors do not exhibit any considerable Re_d-dependent distinctions on the two sides of $\mathrm{Re}_d \approx 10^4$ or $\mathrm{Re}_\lambda \approx 130$. In other words, the regime change of turbulence or the occurrence of any critical Reynolds number is not reflected in the Reynolds number dependence of S or F.

In addition, it should be noted that some previous investigations (e.g., Refs. 55 and 56) showed a decrease of the skewness factor with increasing Re_λ. Such a likely false Re_λ variation of S is believed to result from the measurement error due mainly to the use of an inappropriate (low) cutoff frequency in collecting the velocity signal. This is clearly demonstrated in Fig. 21 with the data of S obtained when using the Kolmogorov frequency $f_K = 207$ Hz at $\mathrm{Re}_d = 4050$ as a single cutoff frequency (f_c) for all the Reynolds numbers.

VI. FURTHER DISCUSSION

The preceding experimental results of Figs. 5–9 and Figs. 12–22, respectively, show differences in global flow characteristics and those in the small-scale turbulence caused due to different Reynolds numbers. Apparently, there is a critical value of Reynolds number (Re_{cr}) below and above which turbulence properties are related with Reynolds number in distinct fashions. In the self-preserving region of the present jet, this critical value is obtained to be $\mathrm{Re}_{d,cr} \approx 1.0 \times 10^4$ for the exit Reynolds number or $\mathrm{Re}_{\lambda,cr} \approx 130$ for the local turbulence Reynolds number which delimits two regimes of turbulence, i.e.,

- Regime (i): partially developed turbulence at $\mathrm{Re}_\lambda < \mathrm{Re}_{\lambda,cr}$, where the energy containing and dissipative scale ranges overlap so that it is viscosity-dependent;
- Regime (ii): fully developed turbulence at $\mathrm{Re}_\lambda \geq \mathrm{Re}_{\lambda,cr}$, where a decoupling has occurred between the small and large scales or the inertial range exists that is independent of viscosity. (This fully developed turbulence should not be considered identical to the Kolmogorov turbulence that refers to an ideal state of turbulence which is locally isotropic and homogeneous, independent of any flows. Note also that the inertial range of the centerline velocity does not really follow the −5/3 power-law even at rather high Reynolds numbers.[51])

It has been proven in Figs. 12 and 13 (and other plots indirectly) that the energy dissipation rate in the present circular jet can be expressed approximately as $\varepsilon \approx K_{\varepsilon l}\nu U_c^2/R^2$ for $\mathrm{Re}_\lambda < \mathrm{Re}_{\lambda,cr}$ in regime (i) and $\varepsilon \approx K_{\varepsilon h}U_c^3/R$ for $\mathrm{Re}_\lambda \geq \mathrm{Re}_{\lambda,cr}$ in regime (ii). It must be acknowledged here that the validity of $\varepsilon \approx K_{\varepsilon h}U_c^3/R$ in the circular jet has also been confirmed via Eq. (6) by several previous investigations such as those reported in Refs. 25 and 36. Nevertheless, the estimate of $K_{\varepsilon h}$ is not identical from the different investigations (e.g., $K_{\varepsilon h} \approx 0.017$ from the present study versus $K_{\varepsilon h} \approx 0.029$ from Ref. 25), perhaps due mainly to distinct jet's initial and boundary conditions.

Besides, Batchelor and Townsend[57] made the first direct attempt, using grid turbulence, to test the validity of the scaling law, which is somehow equivalent to Eq. (5), i.e.,

$$\varepsilon \approx A\langle u^2\rangle^{3/2}/L, \tag{32}$$

where A is a constant for sufficiently high Reynolds number and L is the turbulence integral scale. (Note that this scaling law was originally proposed by Taylor.[58]) It was found that the grid-turbulence data for $\varepsilon L/\langle u^2\rangle^{3/2}$ does not appear to be inconsistent by and large with its constancy over wide ranges of the decay time and Reynolds number, if the constancy of $\varepsilon L/\langle u^2\rangle^{3/2}$ is regarded as an asymptotic expectation. Yet, as noted in Ref. 28, the relatively large scatter in Batchelor's[57] data should be correlated to some Re_λ dependence of $\varepsilon L/\langle u^2\rangle^{3/2}$ at least for $\mathrm{Re}_\lambda \leq 41$. Sreenivasan[28] checked this speculation over a greater range of Re_λ through collecting a number of previous data sets for grid turbulence produced by biplane square meshes, and indeed he found that $\varepsilon L/\langle u^2\rangle^{3/2}$ generally decreases with increasing Reynolds number at $\mathrm{Re}_\lambda < 50$. On the other hand, he also confirmed the good constancy of $\varepsilon L/\langle u^2\rangle^{3/2}$ approximately at $\mathrm{Re}_\lambda \geq 50$. Lately, Mydlarski and Warhaft[49] showed

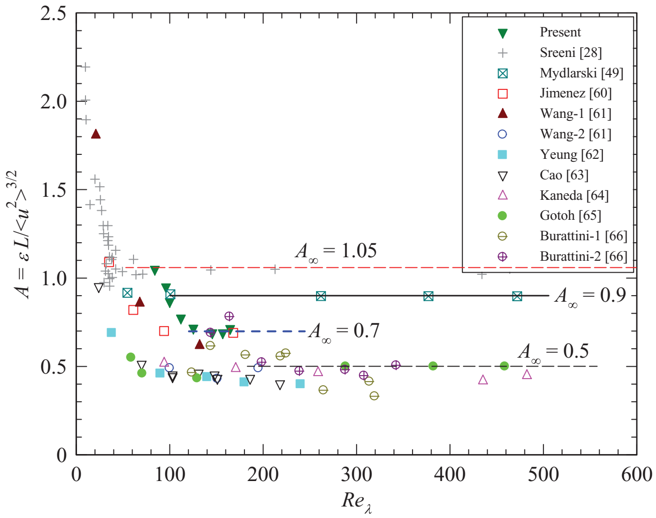

FIG. 23. Dependence of $A = \varepsilon L/\langle u^2\rangle^{3/2}$ on Re_λ. Symbols: ▼, present jet turbulence; +, grid turbulence from biplane square meshes, compiled by Sreenivasan;[28] □, DNS of periodic box turbulence (forced), Jimenez *et al.*;[60] ▲, DNS of periodic box turbulence (decaying), Wang *et al.*;[61] ○, DNS of periodic box turbulence (forced), Wang *et al.*;[61] ■, DNS of periodic box turbulence (forced), Yeung and Zhou;[62] ▽, DNS of periodic box turbulence (forced), Cao *et al.*;[63] Δ, DNS of periodic box turbulence (forced), Kaneda *et al.*;[64] ●, DNS of periodic box turbulence (forced), Gotoh *et al.*;[65] ⊠, grid turbulence generated by active meshes, Mydlarski and Warhaft;[49] ⊖, plate wake, Burattini *et al.*;[66] ⊕, circular cylinder wake, Burattini *et al.*[66]

that the scaling relation applies very well in a slightly different grid turbulence generated by active grid for $\mathrm{Re}_\lambda = 100$–473.

The above findings for grid turbulence, especially that of Sreenivasan,[28] appear to suggest that Eq. (4) for the low-Re_λ regime (i) can be reconciled to Eq. (32) or Eq. (5) so long as A is not treated as being independent of Reynolds number. In fact, re-forming Eq. (4) via the prefactors of Eqs. (1)–(3) obtains that

$$\varepsilon \approx \left(K_{\varepsilon l} K_U^{-1} K_R^{-1} \mathrm{Re}_d^{-1}\right) U_c^3/R = \left(K_{\varepsilon l} K_U^{-1} K_R^{-1} K_I^{-3} C_1 \mathrm{Re}_d^{-1}\right) \left\langle u^2\right\rangle^{3/2}/L \tag{33}$$

and hence that $A = K_{\varepsilon l} K_U^{-1} K_R^{-1} K_I^{-3} C_1 \mathrm{Re}_d^{-1}$ (where $C_1 = L/R$ is correlated with Re_d) for the jet in regime (i). For consistency, Eq. (5) is also converted to the following:

$$\varepsilon \approx \left(K_{\varepsilon h} K_I^{-3} C_1\right) \left\langle u^2\right\rangle^{3/2}/L \tag{34}$$

so that $A = K_{\varepsilon h} K_I^{-3} C_1$ for the jet in regime (ii). Certainly, if reconciling Eqs. (4) and (5) into Eq. (32), the quantity A is a function of Re_d for $\mathrm{Re}_\lambda < \mathrm{Re}_{\lambda,cr}$ since all the quantities but $K_{\varepsilon l}$ in the round brackets of Eq. (33) are dependent on Re_d whereas, distinctly in Eq. (34), K_I, $K_{\varepsilon h}$, and C_1 and thus $A = K_{\varepsilon h} K_I^{-3} C_1$ are all uncorrelated with the Reynolds number for $\mathrm{Re}_\lambda \geq \mathrm{Re}_{\lambda,cr}$. To summarize, Eq. (32) now can be expressed below for the round jet

$$\varepsilon \approx A\frac{\left\langle u^2\right\rangle^{3/2}}{L}, \quad \text{where :} \quad \begin{array}{ll} \text{(i) } A = K_{\varepsilon l} K_U^{-1} K_R^{-1} K_I^{-3} C_1 \mathrm{Re}_d^{-1} & \text{for } \mathrm{Re}_\lambda < \mathrm{Re}_{\lambda,cr}, \\ \text{(ii) } A = K_{\varepsilon h} K_I^{-3} C_1 & \text{for } \mathrm{Re}_\lambda \geq \mathrm{Re}_{\lambda,cr}. \end{array} \tag{32$'$}$$

To check the validity of Eq. (32′) for any Reynolds number of the turbulent jet against grid turbulence, the estimates of $A = \varepsilon L/\langle u^2\rangle^{3/2}$ for the present flow were made for the eight Reynolds numbers of investigation; note that L was determined by a method similar to that of Refs. 28 and 49, i.e., $L \approx 1/k_1 = U_c/2\pi f_o$ where k_1 is the streamwise wavenumber and f_o is the frequency at which a broad peak of frequency times u-spectrum, i.e., $f \cdot \Phi_u$, occurs approximately. The results against Re_λ are presented in Fig. 23 and compared with those for grid turbulence reproduced from Refs. 28 and 49, and for homogeneous turbulence of a periodic box, partly compiled in Ref. 59, from direct numerical simulations (DNS),[60–65] and also for wakes.[66] For $\mathrm{Re}_\lambda < 130$, the present A obviously decreases notably with increasing Re_λ. This variation agrees qualitatively with those of the grid turbulence and the homogeneous (periodic-box) turbulence. The asymptotic value of A (denoted by A_∞) is achieved at $\mathrm{Re}_\lambda \approx 130$ for the present jet; namely, $A = \varepsilon L/\langle u^2\rangle^{3/2}$ becomes nearly independent of Re_λ at $\mathrm{Re}_\lambda \geq 130$. Figure 23 also demonstrates that A_∞ differs appreciably for various flows. Explicitly indicated on the plot are $A_\infty \approx 0.7$ for the present jet and some cases of the homogeneous turbulence,[60,61] $A_\infty \approx 0.5$ for more cases of turbulence,[61–66] $A_\infty \approx 0.9$ for the grid turbulence of Mydlarski and Warhaft,[49] and $A_\infty \approx 1.05$ for that of Sreenivasan[28] (quasi-homogeneous flows) whose data were obtained from a number of previous investigations. The above discrepancies in A_∞ are most likely to result from varying configurations of the large-scale structure in different turbulent flows.[59] Despite A_∞ varying for different flows, according to Fig. 23, $A = \varepsilon L/\langle u^2\rangle^{3/2}$ in general decreases with increasing Re_λ until $\mathrm{Re}_\lambda = \mathrm{Re}_{\lambda,cr}$. When $\mathrm{Re}_\lambda > \mathrm{Re}_{\lambda,cr}$, there is a good constancy of $\varepsilon L/\langle u^2\rangle^{3/2}$, i.e., $A = A_\infty$.

In this context, some comments are worthwhile on the "mixing transition" in turbulent flows proposed by Dimotakis.[24] (Note that the mixing here means the small-scale or molecular mixing.) He found the evidence for the "mixing transition" which occurs, in many free shear flows, within the range of $\mathrm{Re}_L = 10\,000$–$20\,000$ or $\mathrm{Re}_\lambda = 100$–$140$; the large-scale Reynolds number $\mathrm{Re}_L \equiv \langle u^2\rangle^{1/2}L/\upsilon$ where L is the characteristic large-scale length. He regarded this Re_L or Re_λ range as universal and believed that such a transition is the signature of establishing a truly three-dimensional small-scale structure or its occurrence is a necessary requirement for fully developed turbulent flows. He provided an explanation for the "mixing transition" by introducing a new inner length scale l called the laminar-layer thickness. This scale is generated by viscosity after a sweep of size L across the transverse turbulent layer. In the usual hierarchy of turbulent scales, this scale is located in $\eta \ll r \ll l \ll L$, where r represents the smaller scale. It was proposed that a turbulent flow cannot be considered fully developed until the smaller scales are decoupled from those scales of l. Dimotakis[24] utilized the scaling arguments to suggest that the decoupling will not occur until $\mathrm{Re}_\lambda = 100$–$140$. He then indicated that, as Reynolds number increases from a small value to a value approaching some minimum Reynolds number (Re_{min}) for the fully developed turbulence, the jet can generate ever-increasing interfacial area between the mixing species, thereby increasing the smallest-scale mixing rate. He further claimed that, beyond this transition region, i.e., for $\mathrm{Re}_d > \mathrm{Re}_{min}$, the Reynolds number dependence of the amount of mixed fluid can be expected to be weaker. We understand that his Re_{min} is comparable to the critical Reynolds number which defines the border of regimes (i) and (ii).

The present Re_d dependence of the small-scale flow properties appears to support, to some degree, the above claim of Dimotakis.[24] For instance, an increase in Re_d causes the normalized dissipation rate ($\varepsilon d U_j^{-3}$), and hence the smallest-scale mixing rate, to grow approximately linearly for $\mathrm{Re}_d \leq 0.8 \times 10^4$ whereas for $\mathrm{Re}_d > 10^4$ the growth rate becomes nearly invariable (apparently reflected by $\varepsilon d U_j^{-3} \approx$ constant), see Figs. 12 and 13. However, the critical Reynolds number (e.g., $\mathrm{Re}_{\lambda,cr}$) is unlikely to lie in just a narrow range of Reynolds numbers as suggested by Dimotakis[24] generally for any turbulent flows; actually, his suggestion seems incorrect even for similar flows such as round jets issuing from similar-geometry nozzles of different size.[67] His claim that the resulting fully developed turbulence of any flow requires the critical Reynolds number of $\mathrm{Re}_{\lambda,cr} = 100$–$140$ to maintain the state cannot be regarded quite correct, as manifest in Fig. 23. Evidently, a lower value of $\mathrm{Re}_{\lambda,cr} \approx 50$ takes place in the grid turbulence[28] than in the DNS box turbulences[59–64] ($\mathrm{Re}_{\lambda,cr} \approx 90$–$200$) and also in the present jet ($\mathrm{Re}_{\lambda,cr} \approx 130$). Our recent measurements suggest that the fully developed turbulence of a jet from a long square-pipe occurs at $\mathrm{Re}_\lambda > 250$ (not shown here). Furthermore, a number of other experimental investigations[66,68,69] clearly demonstrated that $\mathrm{Re}_{\lambda,cr} \approx 200$–$600$ or even higher, see Fig. 2 of Ref. 65. Hence, we can confidently conclude that, in general, $\mathrm{Re}_{\lambda,cr}$ or the Reynolds number range for the mixing transition should vary from flow to flow and also that the variation range certainly should be greater than that of $100 \leq \mathrm{Re}_{\lambda,cr} \leq 140$.

Moreover, Dimotakis[24] has not made it clear whether the "mixing transition" region in any type of turbulent flows, e.g., turbulent jets, is abrupt or gradual, although it appears to occur within a narrower range of Reynolds numbers than the transition from a steady laminar flow to unsteady fully turbulent flow. Very unfortunately, to our knowledge, previous investigations of the Re_d effect on the small-scale turbulence in a jet (e.g., Refs. 25 and 51) often employed 2-3 greatly different values of Re_d, including none or only one low value ($<10^4$), which are obviously insufficient to determine the "transition region" accurately. This also applies for the study of Fellouah and Pollard[27] who used totally five values of Re_d but only one (i.e., $\mathrm{Re}_d = 6000$) for the case of $\mathrm{Re}_d < 10^4$. The present study, however, used eight Reynolds numbers with four either below or above $\mathrm{Re}_d = 10^4$ and revealed that the "transition region" should occur in the range of $\mathrm{Re}_d = 0.8\times 10^4$–$1.0 \times 10^4$. That is, the mixing transition should be accomplished over a fairly small range of Reynolds numbers.

Important to note as well, the turbulence properties in regime (ii) appear to be affected by the magnitude of the critical Reynolds number. The effect is more evident for low Reynolds number. This may account for the significant departure from 5/3 of the inertial-range exponent (m) of the u spectrum, i.e., $\varphi_u \sim \varepsilon^{2/3}k^{-m}$, see Fig. 8. For the present jets at $\mathrm{Re}_\lambda = 130$–$164$, the exponent was measured to be $m = 1.46$–1.5, versus the asymptotic value of $m = 5/3$ which can be obtained only at much higher values of Re_λ, e.g., at $\mathrm{Re}_\lambda > 1000$ in grid turbulence.[49] It is deduced that, if a change of flow alters the critical Reynolds number, the scaling exponent and perhaps other turbulence properties in regime (ii) will vary. In other words, the fully developed turbulence may be greatly affected by the critical Reynolds number or the onset Reynolds number of the inertial range.

At last, a discussion is worthwhile on the likely effect of initial flow conditions on the critical Reynolds number, which draws up the boundary of regimes (i) and (ii), and the mixing transition of the far-field jet. Mi *et al.*[7] found that both the initial conditions and the near-field structures of the circular jets from the SC and long pipe (LP) nozzles are quite distinct. The SC nozzle, from which the present jets issued, generally produces a "top-hat" (largely uniform) mean velocity profile and a thin (laminar) boundary layer at exit, thus easily generating the natural shear-layer instability and uniform potential core. Consequently, in the near-field region of these jets, well-defined vortical structures are present that exhibit the roll-up, pairing, and break-up process. In contrast, the LP nozzle produces a power-law profile of the mean velocity and a very thick fully turbulent boundary-layer at exit, then resulting in the non-uniform velocity in the "potential core" and the absence of large-scale coherent structures in the near field.[7] Accordingly, one would anticipate that the alteration of Re_d should lead to greater changes of the near-field structure and then the far-field properties in the SC jet than in the LP jet. Indeed, Mi *et al.*[7] demonstrated that the asymptotic centerline decay rate of the mean scalar field of the SC jet depends on Reynolds number while that of the LP jet does not. It is therefore envisaged that, if the exit boundary layer of the present jet were not laminar but turbulent, e.g., issuing from a LP nozzle, the critical Reynolds number would increase in order to maintain the state of the fully developed turbulence, thus resulting in a higher (even slightly) value of the scaling exponent of the velocity spectra.

VII. CONCLUSIONS

This study has successfully clarified by experiments the effect of inflow Reynolds number (Re_d) on typical global and small-scale turbulence properties from the transition region to the (self-preserving) far-field region of a circular jet. The results were obtained for eight Reynolds numbers between $\mathrm{Re}_d = 4050$ and $\mathrm{Re}_d = 20\,100$, with four below and four above $\mathrm{Re}_d = 10^4$. By comparison, to our best knowledge, all previous investigations of the Re_d effect on circular jets (e.g., Refs. 25, 27, and 51) used two to five greatly different values of Re_d, including none or only one low value that is less than $\mathrm{Re}_d = 10^4$. Hence, the present measurements of small-scale turbulence properties may represent closely the true, Re_d-dependent variations of the mean dissipation rate ε, the Kolmogorov length scale η, the Taylor micro-scale λ, although their estimations, as usual, require the assumption of local isotropy and also Taylor's hypothesis. Antonia and Mi[70] and Mi and Antonia[42] found by experiments that both assumptions work well for the scalar dissipation properties along the centerline of the circular jet in the far field. Their results should apply for the energy-dissipation properties. In this sense, based on the analyses provided in Secs. IV–VI, we can draw the following conclusions on the Re_d influence of the present jet flow, some of which may apply generally for any other turbulent flows:

(1) The model of the two Reynolds-number-based regimes of turbulence proposed in, e.g., Tennekes and Lumley,[32] applies well for the circular jet. That is, the critical value for the Taylor microscale Reynolds number (Re_λ) occurs at $\mathrm{R}_{\lambda,cr} \approx 130$ which delimits the following two regimes of turbulence:

- Regime (i): partially developed turbulence at $\mathrm{Re}_\lambda < \mathrm{Re}_{\lambda,cr}$ where the energy containing and dissipative scale ranges overlap so that it is viscosity-dependent;
- Regime (ii): fully developed turbulence at $\mathrm{Re}_\lambda \geq \mathrm{Re}_{\lambda,cr}$, where a decoupling occurs between the small and large scales or the inertial range exists with no viscous effect.

(2) In regime (i), the rates of the mean flow decay and spread (K_U and K_R, see Eqs. (1) and (2)) of the jet vary with Re_d in the forms of $K_U \propto \mathrm{Re}_d^{1/2}$ and $K_R \propto \mathrm{Re}_d^{-1/2}$, but these rates become independent of Re_d in regime (ii).

(3) Distinct fashions of variation with Reynolds number in regimes (i) and (ii) have been found for C_ε, C_η, C_λ and C_{Re}, the prefactors of Eqs. (6)–(10), which formulate the dependences of ε, η, and λ on Re_d and x in the self-similar region.

(4) The mean dissipation rate for the circular jet can be estimated by the centerline velocity (U_c) and half-radius (R) through $\varepsilon \approx K_{\varepsilon l}\nu U_c^2/R^2$ in regime (i) and $\varepsilon \approx K_{\varepsilon h}U_c^3/R$ in regime (ii), where $K_{\varepsilon l} \approx 83$ and $K_{\varepsilon h} \approx 0.016$ from the present measurements. Although the relation for regime (ii) have been well approved by previous measurements in turbulent jets or other turbulent flows, where U_c and R are regarded to represent the characteristic scales, the present study appears to be the first that has experimentally confirmed the relation $\varepsilon \approx K_{\varepsilon l}\nu U_c^2/R^2$, at least in turbulent jets, for regime (i) in detail.

(5) The Re_d dependences of the small-scale properties obtained from the present jet appear to back up the concept of "mixing transition" proposed by Dimotakis.[24] However, the critical Reynolds number for the "mixing transition" in general should be dependent upon both initial and boundary conditions, vary from flow to flow, and vary over a range greater than that of $\mathrm{Re}_{\lambda,cr} = 100$–$140$ as suggested by Dimotakis.[24] In fact, the lower limit of $\mathrm{Re}_{\lambda,cr}$ is revealed to be lower than 100 and the upper limit to be higher than 140.

In addition to the above Reynolds number effects, it is worth noting that the alteration of jet-exit boundary conditions appears to impact notably on the global far-field characteristics but have considerably weaker influence on the fine-scale far-field turbulence in the jet. The present work also suggest that the existence of a power-law range should represent the presence of the inertial range of turbulence no matter whether or not the spectral power-law exponent is $-5/3$, a value which may be reached at extremely high local Reynolds numbers, such as $\mathrm{Re}_\lambda \sim 10^4$ as suggested by Mydlarski and Warhaft[49] based on grid turbulence.

ACKNOWLEDGMENTS

The support of National Science Foundation of China (NSFC) (Grant Nos. 10921202 and 11072005) and the Fundamental Research Funds for the Central Universities (Grant No. 3132013029) are gratefully acknowledged. The authors would also like to thank all the reviewers for their insightful comments and criticisms, the addressing of which has enhanced the paper substantially.

[1] K. R. Sreenivasan and R. A. Antonia, "The phenomenology of small-scale turbulence," Annu. Rev. Fluid Mech. **29**, 435 (1997).
[2] P. E. Dimotakis, "Turbulent mixing," Annu. Rev. Fluid Mech. **37**, 329 (2005).
[3] G. J. Nathan, J. Mi, Z. T. Alwahabi, G. J. R. Newbold, and D. S. Nobes, "Impacts of a jet's exit flow pattern on mixing and combustion performance," Prog. Energy Combust. Sci. **32**, 496 (2006).
[4] G. Batchelor, *The Theory of Homogeneous Turbulence* (Cambridge University Press, 1982).
[5] A. Monin and A. Yaglom, *Statistical Fluid Mechanics* (MIT Press, Cambridge, MA, 1971).
[6] W. K. George, "Self-preservation of turbulent flows and its relation to initial conditions and coherent structures," in *Advances in Turbulence*, edited by W. K. George and R. Arndt (Springer, New York, 1989).
[7] J. Mi, D. S. Nobes, and G. J. Nathan, "Influence of jet exit conditions on the passive scaler field of an axisymmetric free jet," J. Fluid Mech. **432**, 91 (2001).

[8] J. Mi and G. J. Nathan, "Statistical properties of turbulent free jets issuing from nine differently-shaped nozzles," Flow, Turbul. Combust. **84**, 583 (2010).
[9] R. C. Deo, G. J. Nathan, and J. Mi, "Comparison of turbulent jets issuing from a rectangular nozzle with and without sidewalls," Exp. Therm. Fluid Sci. **32**, 596 (2007).
[10] F. P. Ricou and D. B. Spalding, "Measurements of entrainment by axisymmetrical turbulent jets," J. Fluid Mech. **11**, 21 (1961).
[11] P. Dimotakis, R. Miake-Lye, and D. Papantoniou, "Structure and dynamics of round turbulent jets," Phys. Fluids **26**, 3185 (1983).
[12] P. Miller and P. Dimotakis, "Reynolds number dependence of scalar fluctuations in a high Schmidt number turbulent jet," Phys. Fluids A **3**, 1156 (1991).
[13] R. Gilbrech, "An experimental investigation of chemically-reacting, gas-phase turbulent jets," Ph.D. dissertation, California Institute of Technology, 1991.
[14] M. M. Koochesfahani and P. E. Dimotakis, "Mixing and chemical reactions in a turbulent liquid mixing layer," J. Fluid Mech. **170**, 83 (1986).
[15] A. Michalke, "Survey on jet instability theory," Prog. Aerosp. Sci. **21**, 159 (1984).
[16] P. Oosthuizen, "An experimental study of low Reynolds number turbulent circular jet flow," in *Proceedings of the ASME Applied Mechanics, Bioengineering, and Fluids Engineering Conference, Houston, TX*, June 20–22, 1983.
[17] C. Bogey and C. Bailly, "Large eddy simulations of transitional round jets: Influence of the Reynolds number on flow development and energy dissipation," Phys. Fluids **18**, 065101 (2006).
[18] W. M. Pitts, "Reynolds number effects on the mixing behavior of axisymmetric turbulent jets," Exp. Fluids **11**, 135 (1991).
[19] N. R. Panchapakesan and J. L. Lumley, "Turbulence measurements in axisymmetric jets of air and helium. Part 1. Air jet," J. Fluid Mech. **246**, 197 (1993).
[20] H. Hussein, S. Capp, and W. George, "Velocity measurements in a high-Reynolds-number, momentum-conserving, axisymmetric, turbulent jet," J. Fluid Mech. **258**, 31 (1994).
[21] S. B. Pope, *Turbulent Flows* (Cambridge University Press, 2000).
[22] S. J. Kwon and I. W. Seo, "Reynolds number effects on the behavior of a non-buoyant round jet," Exp. Fluids **38**, 801 (2005).
[23] H. Fellouah, C. G. Ball, and A. Pollard, "Reynolds number effects within the development region of a turbulent round free jet," Int. J. Heat Mass Transfer **52**, 3943 (2009).
[24] P. E. Dimotakis, "The mixing transition in turbulent flows," J. Fluid Mech. **409**, 69 (2000).
[25] R. A. Antonia, B. R. Satyaprakash, and A. Hussain, "Measurements of dissipation rate and come other characteristics of turbulent plane and circular jets," Phys. Fluids **23**, 695 (1980).
[26] R. A. Antonia, N. Phan-Thien, and A. J. Chambers, "Taylor's hypothesis and the probability density functions of temporal velocity and temperature derivatives in a turbulent flow," J. Fluid Mech. **100**, 193 (1980).
[27] H. Fellouah and A. Pollard, "The velocity spectra and turbulence length scale distributions in the near to intermediate regions of a round free turbulent jet," Phys. Fluids **21**, 115101 (2009).
[28] K. Sreenivasan, "On the scaling of the turbulence energy dissipation rate," Phys. Fluids **27**, 1048 (1984).
[29] C. W. Van Atta and R. A. Antonia, "Reynolds number dependence of skewness and flatness factors of turbulent velocity derivatives," Phys. Fluids **23**, 252 (1980).
[30] J. Mi, R. C. Deo, and G. J. Nathan, "Fast-convergent iterative scheme for filtering velocity signals and finding Kolmogorov scales," Phys. Rev. E **71**, 066304 (2005).
[31] J. Mi, M. Xu, and C. Du, "Digital filter for hot-wire measurements of small-scale turbulence properties," Meas. Sci. Technol. **22**, 125401 (2011).
[32] H. Tennekes and J. Lumley, *A First Course in Turbulence* (MIT Press, Cambridge, 1972).
[33] A. N. Kolmogorov, "The local structure of turbulence in incompressible viscous fluid for very large Reynolds numbers," Dokl. Akad. Nauk SSSR **30**, 301 (1941).
[34] L. D. Landau and E. M. Lifshitz, *Fluid Mechanics* (Pergamon Press, London, 1959).
[35] A. Townsend, *The Structure of Turbulent Shear Flow* (Cambridge University Press, 1980).
[36] C. Friehe, C. Van Atta, and C. Gibson, "Jet turbulence: Dissipation rate measurements and correlations," AGARD Turbul. Shear Flows **CP-93**, 18.1 (1971).
[37] J. O. Hinze, *Turbulence: An Introduction to its Mechanism and Theory* (McGraw-Hill, New York, 1975).
[38] J. Mi and R. A. Antonia, "Vorticity characteristics of the intermediate turbulent wake," Exp. Fluids **20**, 383 (1996).
[39] J. Wyngaard, "Measurement of small-scale turbulence structure with hot wires," J. Phys. E: J. Sci. Instrum. **1**, 1105 (1968).
[40] R. A. Antonia and J. Mi, "Corrections for velocity and temperature derivatives in turbulent flows," Exp. Fluids **14**, 203 (1993).
[41] R. A. Antonia, D. A. Shah, and L. W. B. Browne, "Spectra of velocity derivatives in a turbulent wake," Phys. Fluids **30**, 3455 (1987).
[42] J. Mi and R. A. Antonia, "Corrections to Taylor hypothesis in a turbulent circular jet," Phys. Fluids **6**, 1548 (1994).
[43] J. Wyngaard and S. Clifford, "Taylor's hypothesis and high-frequency turbulence spectra," J. Atmos. Sci. **34**, 922 (1977).
[44] F. Champagne, "The fine-scale structure of the turbulent velocity field," J. Fluid Mech. **86**, 67 (1978).
[45] G. Wang, N. Clemens, R. Barlow, and P. Varghese, "A system model for assessing scalar dissipation measurement accuracy in turbulent flows," Meas. Sci. Technol. **18**, 1287 (2007).
[46] R. C. Deo, J. Mi, and G. J. Nathan, "The influence of Reynolds number on a plane jet," Phys. Fluids **20**, 075108 (2008).
[47] T. Malmstrom, A. Kirkpatrick, B. Christensen, and K. Knappmiller, "Centreline velocity decay measurements in low-velocity axisymmetric jets," J. Fluid Mech. **346**, 363 (1997).
[48] A. A. Abdel-Rahman, W. Chakroun, and S. F. Al-Fahed, "LDA measurements in the turbulent round jet," Mech. Res. Commun. **24**, 277 (1997).

[49] L. Mydlarski and Z. Warhaft, "On the onset of high-Reynolds-number grid-generated wind tunnel turbulence," J. Fluid Mech. **320**, 331 (1996).
[50] J. Mi and R. A. Antonia, "Effect of large-scale intermittency and mean shear on scaling-range exponents in a turbulent jet," Phys. Rev. E **64**, 026302 (2001).
[51] P. Burattini, R. A. Antonia, and L. Danaila, "Similarity in the far field of a turbulent round jet," Phys. Fluids **17**, 025101 (2005).
[52] G. Lipari and P. K. Stansby, "Review of experimental data on incompressible turbulent round jets," Flow, Turbul. Combust. **87**, 79 (2011).
[53] D. R. Dowling and P. E. Dimotakis, "Similarity of the concentration field of gas-phase turbulent jets," J. Fluid Mech. **218**, 109 (1990).
[54] C. J. Chen and W. Rodi, "Vertical turbulent buoyant jets: A review of experimental data," NASA STI/Recon Tech. Rep. A **80**, 23073 (1980).
[55] C. Richards and W. Pitts, "Global density effects on the self-preservation behaviour of turbulent free jets," J. Fluid Mech. **254**, 417 (1993).
[56] R. W. Stewart, "Triple velocity correlations in isotropic turbulence," Proc. Cambridge Philos. Soc. **47**, 146 (1951).
[57] G. Batchelor and A. Townsend, "Decay of vorticity in isotropic turbulence," Proc. R. Soc.London, Ser. A **190**, 534 (1947).
[58] G. Taylor, "Statistical theory of turbulence," Proc. R. Soc. London, Ser. A **151**, 421 (1935).
[59] K. R. Sreenivasan, "An update on the energy dissipation rate in isotropic turbulence," Phys. Fluids **10**, 528 (1998).
[60] J. Jimenez, A. A. Wray, P. G. Saffman, and R. S. Rogallo, "The structure of intense vorticity in homogeneous isotropic turbulence," J. Fluid Mech. **255**, 65 (1993).
[61] L. P. Wang, S. Chen, J. G. Brasseur, and J. C. Wyngaard, "Examination of hypotheses in the Kolmogorov refined turbulence theory through high-resolution simulations. Part 1. Velocity field," J. Fluid Mech. **309**, 113 (1996).
[62] P. Yeung and Y. Zhou, "Universality of the Kolmogorov constant in numerical simulations of turbulence," Phys. Rev. E **56**, 1746 (1997).
[63] N. Cao, S. Chen, and G. D. Doolen, "Statistics and structures of pressure in isotropic turbulence," Phys. Fluids **11**, 2235 (1999).
[64] Y. Kaneda, T. Ishihara, M. Yokokawa, K. Itakura, and A. Uno, "Energy dissipation rate and energy spectrum in high resolution direct numerical simulations of turbulence in a periodic box," Phys. Fluids **15**, L21 (2003).
[65] T. Gotoh, D. Fukayama, and T. Nakano, "Velocity field statistics in homogeneous steady turbulence obtained using a high-resolution direct numerical simulation," Phys. Fluids **14**, 1065 (2002).
[66] P. Burattini, P. Lavoie, and R. A. Antonia, "On the normalized turbulent energy dissipation rate," Phys. Fluids **17**, 098103 (2005).
[67] J. Mi and C. Du, "Influences of initial velocity, diameter and Reynolds number on a circular turbulent air/air jet," Chin. Phys. B **20**, 124701 (2011).
[68] N. Mazellier and J. C. Vassilicos, "The turbulence dissipation constant is not universal because of its universal dependence on large-scale flow topology," Phys. Fluids **20**, 015101 (2008).
[69] H. Mouri, A. Hori, Y. Kawashima, and K. Hashimoto, "Large-scale length that determines the mean rate of energy dissipation in turbulence," Phys. Rev. E **86**, 026309 (2012).
[70] R. A. Antonia and J. Mi, "Temperature dissipation in a turbulent round jet," J. Fluid Mech. **250**, 531 (1993).